mathematics

MDPI

Article

Dynamic Trust-Driven Resilient Finite-/Fixed-Time Formation Control for Multi-UAV Systems with Input Saturation Against Sybil Attacks

Hanghang Wang [1], Tangxing Liu [1,2], Chuan He [3,*] and Ding Zhou [4,*]

[1] Nanjing Research Institute of Electronic Engineering, No. 99 Houbiaoying Road, Nanjing 210007, China; wangxingxing5@cetc.com.cn (H.W.); liutangxing@cetc.com.cn (T.L.)
[2] Purple Mountain Innovation Center for International Cooperation of Information System Technology, No. 99 Houbiaoying Road, Nanjing 210007, China
[3] School of Cyber Science and Engineering, Southeast University, No. 02 Sipailou, Nanjing 210096, China
[4] Purple Mountain Laboratories, No. 09 Mozhou Road, Nanjing 211111, China
* Correspondence: 230240027@seu.edu.cn (C.H.); zhouding@pmlabs.com.cn (D.Z.)

Abstract

This paper investigates resilient finite-/fixed-time formation control of multi-UAV systems subject to actuator input saturation and Sybil attacks. A dynamic trust-based communication weight is proposed by integrating physical layer confidence assessment, an exponentially discounted trust accumulator, and a smooth nonlinear mapping. The mechanism adaptively updates the adjacency weights, preserves effective information exchange among legitimate UAVs, and gradually suppresses the influence of Sybil-induced links, thereby enabling a self-healing communication topology. Based on the resulting dynamic weighted topology, distributed finite-/fixed-time formation controllers are developed using smooth saturation functions to explicitly accommodate actuator constraints. The finite-time controller ensures formation tracking convergence within a finite settling time, whereas the fixed-time controller guarantees a practical settling-time bound for initial conditions belonging to a prescribed compact set, where the bound may depend on the selected set radius. Lyapunov stability analysis and homogeneity theory are employed to establish closed loop convergence and input boundedness properties. Numerical simulations demonstrate that the proposed approach effectively mitigates malicious communication influences, preserves connectivity among legitimate UAVs, and achieves resilient cooperative formation tracking.

Keywords: resilient formation control; finite/fixed-time stability; sybil attack; input saturation; multi-UAV system

MSC: 93B70; 93D40; 93D50

Check for updates

Received: 16 September 2026
Revised: 22 October 2026
Accepted: 25 October 2026
Published: 29 October 2026

Copyright: © 2026 by the authors. Licensee MDPI, Basel, Switzerland. This article is an open access article distributed under the terms and conditions of the Creative Commons Attribution (CC BY) license.

1. Introduction

Significant progress has been made in multi-agent system (MAS) coordination, motivated by its broad applications in robotic swarms [1], distributed sensor networks [2], and biological collective-behavior modeling [3]. By exploiting local information exchange, MASs enable multiple autonomous agents to accomplish collective tasks in a distributed manner [4]. Among these applications, cooperative unmanned aerial vehicle (UAV) formations have received considerable attention because of their relevance to time-critical missions, including environmental monitoring, aerial reconnaissance, and logistics delivery [5,6]. Such missions require distributed controllers that ensure accurate coordination

and rapid convergence under communication and actuation constraints [7]. Finite-time and fixed-time control are particularly attractive in this context: the former guarantees convergence within a finite settling time, whereas the latter provides a uniform settling-time bound independent of the initial conditions [8,9].

Recent advances in finite- and fixed-time coordination have significantly shaped the development of multi-agent control theory, with a range of analytical frameworks proposed to ensure rapid convergence across diverse operational conditions [10,11]. Despite this progress, notable challenges persist—especially when these strategies are applied to UAV networks deployed in adversarial settings [12]. UAV formations depend on wireless communication to exchange localized state data and coordinate their collective behavior [13]. However, this communication backbone becomes a point of vulnerability, exposing the system to identity spoofing attacks, particularly the Sybil attack [14], where an intruder forges multiple fake identities to disrupt distributed consensus. The impact of such attacks is multifaceted. By impersonating legitimate UAVs, attackers can inject false control signals or positional data, misguiding decision-making processes and impairing coordination [15]. In more severe cases, fake nodes flood the communication network with malicious traffic, degrading bandwidth availability and impeding reliable inter-agent interaction [16]. Moreover, by tampering with the perceived network topology, an attacker can destabilize formation structures, potentially severing communication links and obstructing task execution [17]. To counter these threats, existing techniques often rely on cryptographic methods, computational resource tests, or software-level identity validation [18,19]. While effective in certain contexts, these approaches introduce latency and overhead that are difficult to accommodate in UAV systems constrained by limited computational power and real-time requirements [20,21]. A more promising direction lies in exploiting physical-layer signal features to establish identity trustworthiness without centralized key management [22,23]. Motivated by this observation, this paper incorporates physical-layer confidence evaluations into the distributed control architecture to adapt the interaction weights online and attenuate the influence of Sybil-induced links.

Moreover, actuator saturation constitutes another fundamental limitation in practical UAV formation control. The acceleration or overload commands generated by distributed protocols may exceed the admissible actuator range, particularly in densely connected networks or during large transient maneuvers, thereby causing performance degradation and potentially compromising closed-loop stability [24]. Existing studies have addressed input saturation in finite- or fixed-time control through, for example, nested saturation compensators [25], barrier functions [26], adaptive compensation [27], auxiliary-system-based designs [28], and Nussbaum-function-based methods [29]. However, these approaches generally do not account for Sybil attacks, under which falsified neighbor information can simultaneously corrupt the coordination term and increase the risk of excessive control commands. The situation becomes more complex when such limitations coexist with cyber threats like Sybil attacks [30,31]. In these scenarios, adversaries may forge multiple UAV identities to inject deceptive information or disrupt network communication, further degrading control performance and reliability [32,33].

The interplay between Sybil attacks and actuator saturation creates a tightly coupled challenge that existing methods have yet to comprehensively resolve [34]. Therefore, there is a pressing need for an integrated and resilient control framework that simultaneously addresses actuator saturation, and identity-based attacks within a unified finite-/fixed-time design. Such a framework would mark a significant step toward practical, secure, and robust formation control in UAV networks.

Motivated by the above observations, this paper investigates dynamic trust-driven resilient finite-/fixed-time formation control for multi-UAV systems subject to Sybil attacks and actuator input saturation. The main contributions are summarized as follows.

A dynamic trust-accumulating adjacency-weighting mechanism is developed by combining physical-layer confidence evaluations, exponential forgetting, and a smooth nonlinear mapping. Under the confidence discernibility condition and residual connectivity of the legitimate subgraph, the mechanism preserves positive weights on legitimate links while progressively attenuating the influence of Sybil-induced links.

A distributed finite-time formation controller is constructed using fractional-power saturation functions and dynamic trust-weighted interactions. Sufficient parameter conditions are derived to guarantee finite-time formation tracking while ensuring that the outer-loop acceleration commands comply with the prescribed actuator limits.

A distributed fixed-time formation controller is further developed by integrating bounded hyperbolic-tangent feedback with dynamic trust weight. The proposed controller guarantees a radius-dependent settling-time bound for initial tracking errors belonging to a prescribed compact set, and provides explicit input-boundedness conditions for implementation under actuator saturation.

2. Preliminaries and Problem Formulation

2.1. Notations and Graph Theory

Consider a networked system with undirected communication topology modeled by $G = \{V, \zeta, A\}$, where $V = \{1, 2, \dots, n\}$ is the node set, $\zeta \subseteq \{(i,j) \mid i,j \in V\}$ denotes the edge set, and $A = \left[a_{ij}\right]_{n\times n}$ represents the adjacency matrix satisfying $a_{ii} = 0$ (no self-edges), $a_{ij} = 1$ if $(j,i) \in \zeta$, else $a_{ij} = 0$. The neighborhood of node i is defined as $N_i = \left\{j \in V \mid a_{ij} = 1\right\}$. The nonlinear operator $\mathrm{sig}(\cdot)^\gamma$ is constructed as $\mathrm{sig}(p)^\gamma = \left[\mathrm{sig}(p_1)^\gamma, \dots, \mathrm{sig}(p_n)^\gamma\right]^T$ with element-wise computation rule $\mathrm{sig}(p_i)^\gamma = |p_i|^\gamma \mathrm{sgn}(p_i), \quad \forall i \in V$, where $\mathrm{sgn}(\cdot)$ denotes the signum function. $E[\sigma]$ denotes the Mean value of σ. Key mathematical notations include: identity matrix $I_n \in \mathbb{R}^{n\times n}$, unit vector $\mathbf{1}_n \in \mathbb{R}^n$, Euclidean norm $\|\cdot\|$, and Kronecker product $\otimes$. The graph Laplacian L is generated by $L = D - A$, where the degree matrix $D = \mathrm{diag}\{d_{11}, \dots, d_{nn}\}$ satisfies $d_{ii} = \sum_{j\in V\setminus\{i\}} a_{ij}$. Define $H = diag(a_{10}, a_{20}, \cdots, a_{n0})$ with $a_{i0} > 0$ if the leader is the neighbor of the i-th agent.

2.2. Definition and Lemmas

Definition 1. *Consider the nonlinear dynamical system $\dot{x} = f(x), f(0) = 0, x(0) = x_0, x \in R^n$, where the vector field $f(x) = (f_1(x), \dots, f_n(x)) : U_0 \to R^n$ is continuous on an open neighborhood U_0 containing the origin. Given a dilation vector $(r_1, \dots, r_n) \in R^n$ with strictly positive components $r_i > 0$, the vector field $f(x)$ is called* homogeneous of degree $k \in R$ *if its components satisfy the scaling relationship $\forall \varepsilon > 0,\ \forall x \in R^n, f_i(\varepsilon^{r_1}x_1, \varepsilon^{r_2}x_2, \cdots, \varepsilon^{r_n}x_n) = \varepsilon^{k+r_i} f_i(x)$ for each index $i = 1, \dots, n$. The system is consequently termed homogeneous when its vector field $f(x)$ possesses this homogeneity property.*

Lemma 1 ([35])**.** *Consider the dynamical system governed by $\dot{x} = f(x)$, where x belongs to a set $U \subseteq \mathbb{R}^n$, and U is an open neighborhood containing the origin. Assume that there exists a continuously differentiable and positive definite function $V_1(x) : U \to \mathbb{R}$ that satisfies the following inequality $\dot{V}_1(x) + cV_1(x)^\alpha \le 0, x \in U\setminus\{0\}$, where $c > 0$ and $0 < \alpha < 1$. Under these conditions, the origin is a finite-time stable equilibrium. Additionally, the settling time for this system is bounded by $T \le \frac{V_1(x_0)^{1-\alpha}}{c(1-\alpha)}$.*

Lemma 2 ([36]). *For any w satisfying $w \in (0,1]$, the inequality below can be established.* $\left(\sum_{i=1}^{k}|g_i|\right)^w \le \sum_{i=1}^{k}|g_i|^w \le k^{1-w}\left(\sum_{i=1}^{k}|g_i|\right)^w$, *where* $g_i \in R$.

Lemma 3 ([37]). *Let $V : \mathbb{R}^n \to \mathbb{R}$ be a continuously differentiable, positive definite, proper function, satisfying $\dot{V}(x) \le -\alpha_1 V(x)^{\gamma_1} - \alpha_2 V(x)^{\gamma_2} + \delta_1 V(x)$, for all $x \in \mathbb{R}^n \setminus \{0\}$ along the trajectories of (1) with $\alpha_1, \alpha_2 > 0$, $\delta_1 \in \mathbb{R}$, $\gamma_1 = 1 + \frac{1}{\mu}$, $\gamma_2 = 1 - \frac{1}{\mu}$ for some $\mu > 1$. Then, there exists a neighborhood $D \subseteq \mathbb{R}^n$ of the origin such that for all $x(0) \in D$, the trajectories of $\dot{x} = f(x)$. satisfy $x(t) \in D$ for all $t \ge 0$, and reach the origin within a fixed time T, where*

$$D = \begin{cases} \mathbb{R}^n, & r < 1, \\ \left\{ x \mid V(x) \le k^{\mu}\left(\dfrac{\delta_1 - \sqrt{\delta_1^2 - 4\alpha_1\alpha_2}}{2\alpha_1}\right)^{\mu} \right\}, & r \ge 1, \end{cases}$$

$$T \le \begin{cases} \dfrac{\mu\pi}{2\sqrt{\alpha_1\alpha_2}}, & r \le 0, \\ \dfrac{\mu}{\alpha_1 k_1}\left(\dfrac{\pi}{2} - \tan^{-1} k_2\right), & 0 \le r < 1, \\ \dfrac{\mu k}{(1-k)\sqrt{\alpha_1\alpha_2}}, & r \ge 1, \end{cases}$$

where $r := \dfrac{\delta_1}{2\sqrt{\alpha_1\alpha_2}}$, $0 < k < 1$, $k_1 = \sqrt{\dfrac{4\alpha_1\alpha_2 - \delta_1^2}{4\alpha_1^2}}$ *and* $k_2 = -\dfrac{\delta_1}{\sqrt{4\alpha_1\alpha_2 - \delta_1^2}}$.

Lemma 4 ([38]). *Consider the following system*

$$\dot{x} = f_l(x) + f_g(x) + \hat{f}(x),$$

where $f_l(0) = 0, f_g(0) = 0, \hat{f}(0) = 0, x \in \mathbb{R}^n$. $f_l(x)$ is a continuous homogeneous vector field of degree $k_l < 0$ with respect to the weights $(r_{l_1}, \ldots, r_{l_n})$. $f_g(x)$ is a continuous homogeneous vector field of degree $k_g > 0$ with respect to the weights $(r_{g_1}, \ldots, r_{g_n})$. Assume that $x = 0$ is an asymptotically stable equilibrium of systems $\dot{x} = f_l(x)$ and $\dot{x} = f_g(x)$. Then, $x = 0$ is a locally fixed-time stable equilibrium if

$$\lim_{\varepsilon \to 0} \frac{\hat{f}_i\left(\varepsilon^{r_{l_1}} x_1, \ldots, \varepsilon^{r_{l_n}} x_n\right)}{\varepsilon^{k_l + r_{l_i}}} = 0, \quad i = 1, 2, \ldots, n, \quad \forall x \in S^{n-1} = \{x \in \mathbb{R}^n : \|x\| = 1\}.$$

In addition, if the system $\dot{x} = f_l(x) + f_g(x) + \hat{f}(x)$ is globally asymptotically stable and locally fixed-time stable, then it is globally fixed-time stable.

2.3. Problem Formulation

UAV formation control may be vulnerable to Sybil attacks. During formation flight, UAVs rely on wireless communication to exchange information. An attacker can spoof multiple fake UAV identities and inject false location data, disrupting communication within the formation. This interference can compromise coordinated decision-making, damage the formation's topological structure, and ultimately hinder the successful execution of mission tasks. Moreover, during UAV operation, if the applied control effort exceeds the actuator's allowable thrust or torque capacity, the vehicle's stability may deteriorate, potentially leading to permanent damage in real-world implementations. Therefore, in practical UAV formation control, it is essential to address actuator saturation constraints and Sybil attacks within a unified control framework.

Consider a continuous-time dynamics model of n UAVs (referred to as followers) and a leader (labeled as 0) operating in an adversarial environment, where UAVs communicate

through wireless. In a hierarchical flight-control architecture, the formation controller generates translational acceleration or overload commands, whereas the faster inner-loop autopilot regulates the attitude and tracks these commands. Accordingly, the geometric size and rotational dynamics of each vehicle are not control objectives at the formation-coordination level. As formation control primarily addresses positions and velocities, each UAV can be represented as a point-mass system within the context of formation control [39,40]. The dynamics of each UAV is specified by

$$\begin{cases} \dot{V}_i = g(\eta_{xi}(t) - \sin\theta_i) \\ \dot{\theta}_i = \frac{g}{V_i}\left(\eta_{yi}(t) - \cos\theta_i\right) \\ \dot{\psi}_i = -\frac{g}{V_i \cos\theta_i}\eta_{zi}(t) \\ \eta_{xi} \le \eta_{\max}^x, \eta_{yi} \le \eta_{\max}^y, \eta_{zi} \le \eta_{\max}^z \end{cases} \tag{1}$$

where $\eta_{xi}, \eta_{yi}, \eta_{zi}$ denote correspond to the overload components along the axes of the flight-path coordinate frame, define $\eta_i = \left(\eta_{xi}, \eta_{yi}, \eta_{zi}\right)^T$ as the control input vector, $\eta_{\max}^x, \eta_{\max}^y, \eta_{\max}^z$ are positive constants that represent the physical actuation limit of the UAV, g is the acceleration of gravity, θ_i denotes the flight-path angle, ψ_i is the heading angle, $i = 1, 2, \cdots, n$, V_i represents the speed. The point-mass outer-loop model (1) is singular at $\theta_i = \pm\pi/2$ and $V_i = 0$. Therefore, we assume that the UAV operates in a valid domain satisfying $V_i \ge V_{\min} > 0$ and that θ_i remains sufficiently away from $\pm\pi/2$, so that $\Gamma(\theta_i, \psi_i)$ is invertible. Hence, the mapping involving $\Gamma^{-1} = (1/g)R_i^T$ is well-defined during the closed-loop evolution.

The kinematics of each aerial vehicle are described by

$$\begin{cases} \dot{p}_{xi} = V_i \cos\theta_i \cos\psi_i \\ \dot{p}_{yi} = V_i \sin\theta_i \\ \dot{p}_{zi} = -V_i \cos\theta_i \sin\psi_i \end{cases} \tag{2}$$

where p_{xi}, p_{yi}, p_{zi} denote the position in the earth-fixed inertial coordinate, and define $p_i = \left(p_{xi}, p_{yi}, p_{zi}\right)^T$. Define $v_i = \left(v_{xi}, v_{yi}, v_{zi}\right)^T = (V_i \cos\theta_i \cos\psi_i,\ V_i \sin\theta_i, -V_i \cos\theta_i \sin\psi_i)^T$, where v_{xi}, v_{yi}, v_{zi} represent the components of velocity in the earth-fixed inertial coordinate frame.

The vectors s_i represent the i-th UAV's relative position to the leader and the j-th UAV, respectively. The control objective is to design a distributed control algorithm that enables all UAVs to track the leader while maintaining a desired spatial arrangement. Additionally, the algorithm must address the challenges of input saturation constraints and Sybil attacks. Specifically, $\lim_{t\to T}\|p_i(t) - s_i - p_0(t)\| = 0$, $\lim_{t\to T}\|v_i(t) - v_0(t)\| = 0$ and $\|p_i(t) - s_i - p_0(t)\| = 0$, $\|v_i(t) - v_0(t)\| = 0$ when $t \ge T$, $i, j = 1, 2, \cdots, n$. Here, T denotes a finite or fixed time, $i = 1, 2, \cdots, n$.

3. Main Results

In this section, the problem of finite- and fixed-time formation tracking control under input saturation and Sybil attacks is addressed.

3.1. Dynamic Trust-Accumulating Adjacency Weight Scheme Under Sybil Attacks

In [22], a confidence metric $\sigma_{ij}(t) \in [0, 1]$ was established based on the physical characteristics of wireless signals, utilizing unique radio frequency fingerprinting to distinguish between legitimate and illegitimate nodes for any pair of agents i and j under Sybil attacks. These results demonstrate that the trustworthiness of communicating can be inferred directly from the physical communication signals, indicating that the trust probability between UAVs can be characterized using inherent physical-layer information. Ref. [22] establishes that a metric value of $\sigma_{ij}(t) > 0.5$ for $j \in \mathcal{N}_i$ indicates a legitimate transmission from agent j to agent i, whereas $\sigma_{ij}(t) < 0.5$ for $j \in \mathcal{N}_i$ signifies a malicious transmission.

The critical value $\sigma_{ij}(t) = 0.5$ is completely ambiguous and conveys no definitive trust information regarding the transmission at time t.

Reference [33] constructs link weights directly from the instantaneous confidence metric (i.e., a memoryless snapshot mapping) and combines an event-triggered mechanism to study resilient fixed-time consensus/flocking for mobile sensor networks. Its focus is primarily on event-triggered communication and the handling of input delay. However, directly employing a memoryless snapshot thresholding rule on $\sigma_{ij}(t)$ suffers from fundamental limitations in multi-UAV formation control. In practical aerial wireless environments, the instantaneous measurements $\sigma_{ij}(t)$ are inevitably corrupted by multipath fading, Doppler shifts, and stochastic channel noise. Consequently, instantaneous thresholding can trigger false alarms in which legitimate communication links are intermittently severed, thereby inducing high-frequency topological chattering and transient loss of network connectivity. A memoryless metric fails to preserve historical attack evidence, rendering the formation system vulnerable to sophisticated Sybil nodes that strategically oscillate near the neutral threshold. Directly mapping the instantaneous confidence metric without dynamic accumulation of historical evidence may lead to high-frequency fluctuations of adjacency weights under stochastic channel noise.

To address these issues, we formulate a continuous-time dynamic trust accumulation equation incorporating a smoothed hyperbolic tangent mapping to update communication weights. Under the conditions of trust mean distinguishability and independent sampling, we employ the Chernoff–Hoeffding inequality to bound the deviation of the trust state at specific sampling instants, thereby quantifying the reliability guarantees for legitimate link weights and the suppression of Sybil links. Consider the scenario where a subset of UAVs, with indices denoted by the set $M \subset V$, is either malicious or malfunctioning. The set $\mathcal{M}$ is assumed to be unknown. A UAV that is neither malicious nor malfunctioning is termed legitimate, and the set of legitimate agents is denoted by $\Lambda \subset V$ ($V = \Lambda \cup M$, $\Lambda \cap M = \emptyset$).

We next present the assumptions utilized in the subsequent analysis. To this end, let $G_\Lambda = (\Lambda, \zeta_\Lambda)$ denote the subgraph of G induced by the legitimate UAVs, where $\zeta_\Lambda \subset \zeta$ is defined as $\zeta_\Lambda = \{(i,j) \in \zeta \mid i \in \Lambda, j \in \Lambda\}$. The following assumptions are maintained throughout this article.

Assumption 1. *Suppose that the following conditions hold:*

(1) The subgraph G_Λ induced by the legitimate UAVs is connected, and at least one legitimate follower retains access to the leader's state information.

(2) For each evaluated communication link, the physical-layer confidence observations are obtained at sampling instants $t_k = kT_s$ and denoted by $\sigma_{ij}[k] \in [0,1]$, where $T_s > 0$ is the sampling period. Within the analyzed interval of unchanged statistical conditions, the observation sequence for each link is independent and identically distributed over time.

Assumption 2. *For each communication link (j,i), there exist constants $T_0 \geq 0$, $c > 0$, $\bar{\Delta} > 0$, and a limit value $\sigma_{ij}^* \in [0,1]$ such that $|\sigma_{ij}(t) - \sigma_{ij}^*| \leq \bar{\Delta} e^{-c(t-T_0)}$, $\forall t \geq T_0$. Moreover, this bound holds simultaneously for all links used in the stability analysis.*

Lemma 5 ([14,22])**.** *The physical-layer confidence evaluation metric $\sigma_{ij}(t) \in [0,1]$ satisfies the discernibility condition, where a metric value of $\sigma_{ij}(t) > 0.5$ for $j \in \mathcal{N}_i$ indicates a legitimate transmission from agent j to agent i, whereas $\sigma_{ij}(t) < 0.5$ for $j \in \mathcal{N}_i$ signifies a malicious transmission. Specifically, there exist positive constants $d_{\min} \in (0, 1/2]$ and $c_{\min} \in (0, 1/2]$ such that*

$$\begin{cases} \mathbb{E}[\sigma_{ij}(t)] \geq \frac{1}{2} + d_{\min}, & \forall j \in \Lambda \\ \mathbb{E}[\sigma_{im}(t)] \leq \frac{1}{2} - c_{\min}, & \forall m \in M \end{cases} \tag{3}$$

To suppress high-frequency physical-layer measurement noise while preserving historical evidence under uninformative baseline conditions, we develop a continuous-time dynamic trust accumulation state $\beta_{ij}(t) \in \mathbb{R}$ for each communication link (j,i) of UAV i, which is governed by the following continuous differential equation

$$\dot{\beta}_{ij}(t) = -\lambda\beta_{ij}(t) + \left(\sigma_{ij}(t) - \frac{1}{2}\right), \quad \beta_{ij}(0) = 0, \tag{4}$$

where $\lambda > 0$ denotes an exponential forgetting rate. The explicit continuous-time integral solution of (4) is

$$\beta_{ij}(t) = \int_0^t e^{-\lambda(t-\tau)}\left(\sigma_{ij}(\tau) - \frac{1}{2}\right)d\tau. \tag{5}$$

The confidence input is held constant over each sampling interval, namely, $\sigma_{ij}(t) = \sigma_{ij}[k]$ for $t \in [kT_s, (k+1)T_s)$. Let $q = e^{-\lambda T_s}$. From (5), at $t_N = NT_s$, $\beta_{ij}(t_N) = \sum_{k=0}^{N-1} w_{N,k}\left(\sigma_{ij}[k] - \frac{1}{2}\right)$, $w_{N,k} = \frac{1-q}{\lambda}q^{N-1-k}$. For notational convenience, define the weight $S_N = \sum_{k=0}^{N-1} w_{N,k} = \frac{1-q^N}{\lambda}$, the sum of squares of weights $Q_N = \sum_{k=0}^{N-1} w_{N,k}^2 = \frac{(1-q)^2}{\lambda^2}\frac{1-q^{2N}}{1-q^2}$, $h_N(\delta) = \sqrt{\frac{Q_N}{2}\ln\frac{1}{\delta}}$, $N \geq 1$, $\delta \in (0,1)$.

To avoid discontinuous switching that would destroy the continuous differentiability of Lyapunov functions in non-linear stability proofs, the dynamic trust state $\beta_{ij}(t)$ is mapped to the dynamic trust-accumulating adjacency matrix weight $a_{ij}(t)$ via a strictly increasing hyperbolic-tangent function:

$$a_{ij}(t) = a_{\max}\cdot\left[\frac{1}{2} + \frac{1}{2}\tanh\left(k_\beta\beta_{ij}(t)\right)\right] a_{ij}(t) = \frac{a_{\max}}{1+\exp\left(-2k_\beta\beta_{ij}(t)\right)}, \quad \forall j \in \mathcal{N}_i, \tag{6}$$

where $a_{\max} > 0$ denotes the nominal communication link weight and $k_\beta > 0$ is a tuning slope gain.

Theorem 1. *Consider the multi-UAV communication network with the legitimate node set Λ and the Sybil node set M. Suppose that the physical-layer confidence evaluation metric satisfies Assumption 1. Under the dynamic adjacency weighting mechanism governed by (4)–(6), the following two properties hold:*

(1) For every legitimate edge (j,i) with $i,j \in \Lambda$, the dynamic adjacency weight $a_{ij}(t)$ satisfies $a_{ij}(t) \geq a_{\min} := \frac{a_{\max}}{1+\exp(k_\beta/\lambda)} > 0$, $t \geq 0$. Furthermore, for any specified sampling instant t_N and $\delta \in (0,1)$, $\Pr\left[a_{ij}(t_N) \geq \frac{a_{\max}}{1+\exp\{-2k_\beta[d_{\min}S_N - h_N(\delta)]\}}\right] \geq 1-\delta$.

(2) For every evaluated incoming link from a Sybil node $m \in M$ to a legitimate node $i \in \Lambda$, $\Pr\left[a_{im}(t_N) \leq \frac{a_{\max}}{1+\exp\{2k_\beta[c_{\min}S_N - h_N(\delta)]\}}\right] \geq 1-\delta$. If $b_N := c_{\min}S_N - h_N(\delta) > 0$, then, for any prescribed tolerance $\epsilon \in (0, a_{\max}/2)$, choosing $k_\beta \geq \frac{\ln(a_{\max}/\epsilon - 1)}{2b_N}$ ensures $\Pr[a_{im}(t_N) \leq \epsilon] \geq 1-\delta$.

Proof. From (5), taking the mathematical expectation on both sides yields

$$\mathbb{E}\left[\beta_{ij}(t)\right] = \int_0^t e^{-\lambda(t-\tau)}\mathbb{E}\left[\sigma_{ij}(\tau) - \frac{1}{2}\right]d\tau. \tag{7}$$

For any legitimate neighbor $j \in \Lambda$, according to Lemma 5, it holds that

$$\mathbb{E}\left[\beta_{ij}(t)\right] \geq d_{\min}\int_0^t e^{-\lambda(t-\tau)}d\tau = \frac{d_{\min}}{\lambda}\left(1 - e^{-\lambda t}\right) > 0. \tag{8}$$

In particular, at $t_N = NT_s$, $\mathbb{E}[\beta_{ij}(t_N)] \geq d_{\min}S_N$. By the sampled representation, $\beta_{ij}(t_N)$ is a weighted sum of independent bounded random variables. The kth weighted term,

$w_{N,k}(\sigma_{ij}[k]-1/2)$, has a range of length $w_{N,k}$. Therefore, the one-sided Chernoff–Hoeffding inequality gives, for any $x>0$,

$$\Pr\Big[\beta_{ij}(t_N)-\mathbb{E}[\beta_{ij}(t_N)]\le -x\Big]\le \exp\Big(-\frac{2x^2}{Q_N}\Big). \tag{9}$$

Setting $x = h_N(\delta)$ and using the expectation bound for legitimate links yields $\Pr\Big[\beta_{ij}(t_N)\ge d_{\min}S_N - h_N(\delta)\Big]\ge 1-\delta$.

Conversely, for any Sybil node $m\in M$, conditions (3) and (5) imply

$$\mathbb{E}[\beta_{im}(t)]\le -c_{\min}\int_0^t e^{-\lambda(t-\tau)}d\tau = -\frac{c_{\min}}{\lambda}\big(1-e^{-\lambda t}\big)<0, \tag{10}$$

and hence $\mathbb{E}[\beta_{im}(t_N)]\le -c_{\min}S_N$. Applying the corresponding upper-tail Chernoff–Hoeffding bound $\Pr[\beta_{im}(t_N)-\mathbb{E}[\beta_{im}(t_N)]\ge x]\le \exp\Big(-\frac{2x^2}{Q_N}\Big)$, we obtain

$$\Pr[\beta_{im}(t_N)\le -c_{\min}S_N + h_N(\delta)]\ge 1-\delta. \tag{11}$$

Define the mapping function $f(x)\triangleq \frac{a_{\max}}{1+\exp(-2k_\beta x)}$. Since $f'(x)=\frac{2k_\beta a_{\max}\exp(-2k_\beta x)}{(1+\exp(-2k_\beta x))^2}>0$, applying f to the one-sided trust-state bounds. To establish the deterministic lower bound for legitimate weights, $\sigma_{ij}(t)\in[0,1]$ and (5) give

$$|\beta_{ij}(t)|\le \frac{1}{2}\int_0^t e^{-\lambda(t-\tau)}d\tau = \frac{1-e^{-\lambda t}}{2\lambda}\le \frac{1}{2\lambda}. \tag{12}$$

Thus, $a_{ij}(t)\ge f(-1/(2\lambda)) = a_{\min}>0$. For the legitimate undirected subgraph with persistent candidate edges and symmetric weights, $L_\Lambda(t)\ge a_{\min}L_\Lambda^{\text{nominal}}$, which yields the stated algebraic connectivity bound. Consequently, $\lambda_2(L_\Lambda(t))\ge a_{\min}\lambda_2(L_\Lambda^{\text{nominal}})>0$, where $L_\Lambda^{\text{nominal}}$ is the Laplacian of the legitimate candidate subgraph with unit edge weights.

Finally, when $b_N>0, f(-b_N)=\frac{a_{\max}}{1+\exp(2k_\beta b_N)}\le\epsilon$ is equivalent to $k_\beta\ge\frac{\ln(a_{\max}/\epsilon-1)}{2b_N}$. Together with the probabilistic bound for the malicious trust state, this proves statements. This completes the proof. □

Remark 1. *The probability bound in Theorem 1 applies to specific sampling instants and does not imply that the belief state converges to a deterministic constant with probability 1. For fixed $\lambda>0$ and $T_s>0$ (letting $q=e^{-\lambda T_s}$), we have $Q_N\longrightarrow\frac{1-q}{\lambda^2(1+q)}>0$ and $\frac{S_N^2}{Q_N}\longrightarrow\frac{1+q}{1-q}<\infty$. Consequently, for a given deviation threshold, the magnitude of the exponential term in the concentration bound remains bounded; the resulting upper bound on the misclassification probability does not simply vanish as time progresses. These bounds do not establish a property of convergence with probability 1. When the conditions of Theorem 1 are met, malicious link suppression using a finite k_β value manifests as the link weight decaying below a preset positive tolerance with probability at least $1-\delta$, rather than achieving isolation through weights becoming exactly zero.*

Under Assumption 2, define $z_{ij}(t)=\sigma_{ij}(t)-\frac{1}{2}$, $z_{ij}^*=\sigma_{ij}^*-\frac{1}{2}$, and $\beta_{ij}^*=z_{ij}^*/\lambda$. Define errors $\tilde\beta_{ij}=\beta_{ij}-\beta_{ij}^*$, $\tilde a_{ij}=a_{ij}-a_{ij}^*$, where a_{ij}^*,β_{ij}^* are positive constants. Then there exists a constant $M_\beta>0$ and $\mu=\min\{\lambda,c\}>0$ such that $|\beta_{ij}(t)-\beta_{ij}^*|\le M_\beta e^{-\mu(t-T_0)}, \quad \forall t\ge T_0$. Also, since $\frac{da_{ij}}{d\beta}=\frac{2k_\beta a_{\max}e^{-2k_\beta\beta}}{\left(1+e^{-2k_\beta\beta}\right)^2}\le\frac{k_\beta a_{\max}}{2}$, we obtain $|a_{ij}(t)-a_{ij}^*|\le\frac{k_\beta a_{\max}}{2}M_\beta e^{-\mu(t-T_0)}$.

Using the variation-of-constants formula for the stable linear system, $\tilde\beta_{ij}(t)=e^{-\lambda(t-T_0)}\tilde\beta_{ij}(T_0)+\int_{T_0}^t e^{-\lambda(t-\tau)}\big(z_{ij}(\tau)-z_{ij}^*\big)d\tau$, hence for $t\ge T_0$, $|\tilde\beta_{ij}(t)|\le e^{-\lambda(t-T_0)}|\tilde\beta_{ij}(T_0)|+\bar\Delta e^{-\lambda(t-T_0)}\int_{T_0}^t e^{(\lambda-c)(\tau-T_0)}d\tau$. If $c\neq\lambda$, the integral yields a bound of the form $|\tilde\beta_{ij}(t)|\le M_\beta e^{-\mu(t-T_0)}, \quad \mu=\min\{\lambda,c\}$, for some constant $M_\beta>0$. Consequently, $|\dot\beta_{ij}(t)|\le\lambda|\tilde\beta_{ij}(t)|+|u_{ij}(t)-u_{ij}^*|\le(\lambda M_\beta+\bar\Delta)e^{-\mu(t-T_0)}$.

Next, consider the logistic mapping $a_{ij}(t) = \frac{a_{\max}}{1+\exp(-2k_\beta\beta_{ij}(t))}$. Let $x = \exp(-2k_\beta\beta_{ij}(t)) > 0$. Then $\frac{da_{ij}}{d\beta_{ij}} = \frac{2k_\beta a_{\max} x}{(1+x)^2} \le \frac{k_\beta a_{\max}}{2}$, since $\max_{x>0} \frac{x}{(1+x)^2} = \frac{1}{4}$. Therefore, $|\dot{a}_{ij}(t)| = \left|\frac{da_{ij}}{d\beta_{ij}}\dot{\beta}_{ij}(t)\right| \le \frac{k_\beta a_{\max}}{2}(\lambda M_\beta + \bar{\Delta})e^{-\mu(t-T_0)}$.

For any prescribed $\varepsilon_d > 0$, choosing $T_{\text{trust}} = T_0 + \frac{1}{\mu}\ln\left(\frac{\frac{k_\beta a_{\max}}{2}(\lambda M_\beta+\bar{\Delta})}{\varepsilon_d}\right)$ guarantees that, for all $t \ge T_{trust}$, $|\dot{a}_{ij}(t)| \le \varepsilon_d$, $|a_{ij}(t) - a^*_{ij}| \le \frac{M_\beta \varepsilon_d}{2(\lambda M_\beta+\bar{\Delta})}$.

The gain k_β determines the steepness of the trust-to-weight mapping. For finite k_β, the mapping is continuous; however, a large gain narrows the transition region around zero trust and can produce near-switching weight behavior. Along the filter trajectories, almost everywhere, $\dot{a}_{ij}(t) = \frac{a_{\max}k_\beta}{2}\operatorname{sech}^2\left(k_\beta\beta_{ij}(t)\right)\dot{\beta}_{ij}(t)$. The maximum mapping slope, attained at $\beta_{ij} = 0$, is therefore $a_{\max}k_\beta/2$. Increasing k_β reduces malicious-link weights for negative trust states but increases weight sensitivity near zero. For a given confidence process, k_β does not change the trust-sign misclassification probability, and every gain gives $a_{ij} = a_{\max}/2$ at $\beta_{ij} = 0$. Gain selection should therefore account jointly for the target weight tolerance, the probability margin, and the observed weight-change rate, rather than relying solely on continuity or saturation of the mapping.

3.2. Finite-Time Formation Control Subject to Sybil Attacks and Input Saturation

Due to the saturation characteristics of physical actuators, input constraints are common in UAV systems during practical applications. This issue becomes particularly significant in complex connectivity topologies. To deal with the input saturation problem, the below saturation function is introduced by

$$s^\alpha_\gamma(v) = \begin{cases} sig(v)^\alpha, |v| < \gamma \\ \frac{\gamma^\alpha sig(v)^\alpha}{|v|^\alpha}, |v| \ge \gamma \end{cases} \tag{13}$$

where $\alpha > 0$, $\gamma > 0$, $v \in R$. Define $s^\alpha_\gamma(\mathrm{Y}) = \left[s^\alpha_{\gamma_1}(v_1), s^\alpha_{\gamma_2}(v_2), s^\alpha_{\gamma_3}(v_3)\right]^T$, $\mathrm{Y} = [v_1, v_2, v_3]^T$.

Consider the radially unbounded function defined by

$$S^\alpha_\gamma(v) = \begin{cases} \frac{|v|^{\alpha+1}}{\alpha+1}, |v| < \gamma \\ \gamma^\alpha|v| - \frac{\alpha\gamma^{\alpha+1}}{\alpha+1}, |v| \ge \gamma \end{cases} \tag{14}$$

The time derivative of $S^\alpha_\gamma(v)$ is $\frac{dS^\alpha_\gamma(v)}{dt} = s^\alpha_\gamma(v)$. Define $S^\alpha_\gamma(\mathrm{Y}) = [S^\alpha_{\gamma_1}(v_1), S^\alpha_{\gamma_2}(v_2), S^\alpha_{\gamma_3}(v_3)]^T$, $\mathrm{Y} = [v_1, v_2, v_3]^T$.

By differentiating the Earth-fixed inertial velocity vector $v_i = (v_{xi}, v_{yi}, v_{zi})^T = (V_i\cos\theta_i\cos\psi_i, V_i\sin\theta_i, -V_i\cos\theta_i\sin\psi_i)^T$ with respect to time, we obtain

$$\begin{cases} \dot{v}_{xi} = g\cos\theta_i\cos\psi_i\eta_{xi}(t) - g\sin\theta_i\cos\psi_i\eta_{yi}(t) + g\sin\psi_i\eta_{zi}(t) \\ \dot{v}_{yi} = -g + g\sin\theta_i\eta_{xi}(t) + g\cos\theta_i\eta_{yi}(t) \\ \dot{v}_{zi} = -g\cos\theta_i\sin\psi_i\eta_{xi}(t) + g\sin\theta_i\sin\psi_i\eta_{yi}(t) + g\cos\psi_i\eta_{zi}(t) \end{cases} \tag{15}$$

The gravity term is moved to the left-hand side of the equation and formulated in compact matrix form.

$$\begin{pmatrix} \dot{v}_{xi} \\ \dot{v}_{yi} + g \\ \dot{v}_{zi} \end{pmatrix} = \Gamma(\theta_i, \psi_i)\begin{pmatrix} \eta_{xi}(t) \\ \eta_{yi}(t) \\ \eta_{zi}(t) \end{pmatrix} \tag{16}$$

where $\Gamma(\theta_i, \psi_i) = g \bullet R_i(\theta_i, \psi_i)$, $R_i(\theta_i, \psi_i) = \begin{bmatrix} \cos\theta_i\cos\psi_i & -\sin\theta_i\cos\psi_i & \sin\psi_i \\ \sin\theta_i & \cos\theta_i & 0 \\ -\cos\theta_i\sin\psi_i & \sin\theta_i\sin\psi_i & \cos\psi_i \end{bmatrix}$.

The matrix R_i is the direction-cosine rotation matrix that transforms coordinates from the flight-path coordinate frame to the earth-fixed inertial coordinate frame. Owing to

its orthogonality, we have $R_i^T R_i = I$ and $R_i^{-1} = R_i^{\mathrm{T}}$. The inverse mapping is given by $\Gamma^{-1}(\theta_i, \psi_i) = \frac{1}{g} R_i^{\mathrm{T}}(\theta_i, \psi_i)$. To achieve finite-time tracking control for all followers, the following distributed control input is developed using the dynamic adjacency matrix weight (6) and saturation function (13)

$$\begin{aligned}
\begin{pmatrix} \eta_{xi}(t) \\ \eta_{yi}(t) \\ \eta_{zi}(t) \end{pmatrix} &= \frac{1}{g} \begin{bmatrix} \cos\theta_i \cos\psi_i & \sin\theta_i & -\cos\theta_i \sin\psi_i \\ -\sin\theta_i \cos\psi_i & \cos\theta_i & 0 \\ \sin\psi_i & 0 & \cos\psi_i \end{bmatrix} \begin{pmatrix} \dot{v}_{xi} \\ \dot{v}_{yi} + g \\ \dot{v}_{zi} \end{pmatrix} \\
\begin{pmatrix} \dot{v}_{xi} \\ \dot{v}_{yi} \\ \dot{v}_{zi} \end{pmatrix} &= -k_1 s_{\gamma_1}^{\alpha_1} \left(\sum_{j=1}^{n} a_{ij}(t) \left((p_i - s_i) - \left(p_j - s_j \right) \right) + a_{i0}(t)(p_i - s_i - p_0) \right) \\
&\quad - k_2 s_{\gamma_1}^{\alpha_2} \left(\sum_{j=1}^{n} a_{ij}(t)(v_i - v_j) + a_{i0}(t)(v_i - v_0) \right) + s_{\gamma_2}^{1}\left(\ddot{o}_{pi} \right)
\end{aligned} \tag{17}$$

where $s_{\gamma_1}^{\alpha_1}(p) = \left(s_{\gamma_{x1}}^{\alpha_1}(p_x), s_{\gamma_{y1}}^{\alpha_1}\left(p_y\right), s_{\gamma_{z1}}^{\alpha_1}(p_z) \right)^T$, $s_{\gamma_1}^{\alpha_2}(p) = \left(s_{\gamma_{x1}}^{\alpha_2}(p_x), s_{\gamma_{y1}}^{\alpha_2}\left(p_y\right), s_{\gamma_{z1}}^{\alpha_2}(p_z) \right)^T$, $s_{\gamma_2}^{1}(p) = \left(s_{\gamma_{x2}}^{1}(p_x), s_{\gamma_{y2}}^{1}\left(p_y\right), s_{\gamma_{z2}}^{1}(p_z) \right)^T$, $\gamma_{x1}, \gamma_{y1}, \gamma_{z1}, \gamma_{x2}, \gamma_{y2}, \gamma_{z2} > 0$, $k_1 > 0$, $k_2 > 0$, $\alpha_1 \in (0,1)$, $\alpha_2 = \frac{2\alpha_1}{1+\alpha_1}$. o_{pi} represents the i agent's estimate of the leader, $\dot{o}_{pi} = \frac{\sum_{j=0}^{n} a_{ij}\dot{o}_{pj}}{\sum_{j=0}^{n} a_{ij}} - \frac{k_3}{\sum_{j=0}^{n} a_{ij}} sig\left(\sum_{j=0}^{n} a_{ij}\left(o_{pi} - o_{pj}\right) \right)^{z_1/s_1} - \frac{k_4}{\sum_{j=0}^{n} a_{ij}} sig\left(\sum_{j=0}^{n} a_{ij}\left(o_{pi} - o_{pj}\right) \right)^{z_2/s_2}$, $o_{p0} = p_0$, where $k_3, k_4 > 0$, z_1, s_1, z_2, s_2 positive odd numbers, $z_1 > s_1, z_2 < s_2$. The estimation mechanism guarantees convergence to the leader's dynamic states within a predetermined time $T_1 \le \frac{1}{\sqrt{z_1 s_1}^{1-z_1/s_1} k_3} \frac{s_1}{z_1 - s_1} + \frac{1}{k_4} \frac{s_2}{s_2 - z_2}$. Detailed theoretical analysis can be seen in our previous work [40].

Next, we demonstrate that the control algorithm (10) is bounded and satisfies the input saturation constraints. Considering the UAV's flight-path angle θ_i and heading angle ψ_i, the triaxial accelerations must satisfy the following inequality

$$\begin{cases} \left| \cos\theta_i \cos\psi_i \cdot \dot{v}_{xi} + \sin\theta_i \cdot (\dot{v}_{yi} + g) - \cos\theta_i \sin\psi_i \cdot \dot{v}_{zi} \right| \le g\eta_{\max}^{x} \\ \left| -\sin\theta_i \cos\psi_i \cdot \dot{v}_{xi} + \cos\theta_i \cdot (\dot{v}_{yi} + g) + \sin\theta_i \sin\psi_i \cdot \dot{v}_{zi} \right| \le g\eta_{\max}^{y} \\ \left| \sin\psi_i \cdot \dot{v}_{xi} + \cos\psi_i \cdot \dot{v}_{zi} \right| \le g\eta_{\max}^{z} \end{cases} \tag{18}$$

This boundary condition (18) is the most precise, as it directly applies the overload component constraints to the acceleration components transformed by the current attitude angles (θ_i, ψ_i). However, formation control typically only focuses on generating a desired inertial frame acceleration command, without directly relying on the UAV's real-time attitude angles. To ensure that the inner-loop overload components do not exceed their limits regardless of how the UAV maneuvers (i.e., irrespective of the values of θ_i and ψ_i), the outer-loop formation control command must be restricted to a more conservative, yet attitude-independent, range.

First, we identify the minimum among the three axial overload limits, defined as $\eta_{\min} = \min\{\eta_{\max}^{x}, \eta_{\max}^{y}, \eta_{\max}^{z}\}$. To ensure that the overload components do not exceed their limits in any attitude, the acceleration command output by the outer-loop controller should be restricted to the following range

$$\begin{cases} |\dot{v}_{xi}| \le k_1 \gamma_1^{\alpha_1} + k_2 \gamma_1^{\alpha_2} + \gamma_2 \le \frac{g}{\sqrt{3}} \eta_{\min} \\ |\dot{v}_{iy} + g| \le k_1 \gamma_1^{\alpha_1} + k_2 \gamma_1^{\alpha_2} + \gamma_2 \le \frac{g}{\sqrt{3}} \eta_{\min} \\ |\dot{v}_{zi}| \le k_1 \gamma_1^{\alpha_1} + k_2 \gamma_1^{\alpha_2} + \gamma_2 \le \frac{g}{\sqrt{3}} \eta_{\min} \end{cases} \tag{19}$$

When designing the outer-loop acceleration control $\dot{v}_{xi}, \dot{v}_{yi}, \dot{v}_{zi}$, we apply saturation functions (13) to the desired acceleration for each axis, ensuring that their output values are

confined within the previously derived range through the selection of control parameters, thereby effectively mitigating input saturation induced by neighbor population growth.

Theorem 2. *Consider a networked system (1) (2) containing n follower UAVs and one leader UAV. Under Assumption 1, the finite-time control algorithm (17) is developed using the confidence weight (6), and the saturation function (13). The finite-time tracking control problem, accounting for input saturation and Sybil attacks, can be solved using the proposed method, provided that the parameters satisfy:*

$$\alpha_1 \in (0,1), \alpha_2 = \frac{2\alpha_1}{1+\alpha_1}$$

$$k_1 > \max\left\{ c\frac{\alpha_1+1}{\gamma_1^{\alpha_1}}\left(\frac{2\rho}{3\lambda_{\min}}\right)^{\frac{2}{3}}, k_2\gamma_1^{\alpha_2-\alpha_1}\sqrt{3n}, 2^{\frac{2(1+\alpha_1)}{3+\alpha_1}}\left(\frac{\rho(1+\alpha_1)\sqrt{2\lambda_{\max}}}{(3+\alpha_1)\lambda_{\min}}\right)^{1+\alpha_1} \right\}$$

$$k_2 > \frac{\rho(1+\alpha_1)\sqrt{2\lambda_{\max}}}{3\lambda_{\min}\gamma_1^{\alpha_1}\left(\sqrt{3}-1\right)}$$

Furthermore, $\gamma_{x1}, \gamma_{y1}, \gamma_{z1}, \gamma_{x2}, \gamma_{y2}, \gamma_{z2}$ should be chosen in accordance with the actuator's saturation (19) limit to ensure operational feasibility.

Proof. In the Earth-fixed inertial coordinate frame, the formation control system described by (1) (2) and (17) can be rewritten as

$$\begin{aligned}
\dot{p}_i =& q_i \\
\dot{q}_i =& -k_1 s_{\gamma_1}^{\alpha_1}\left(\sum_{j=1}^{n} a_{ij}(t)\left((p_i - s_i) - \left(p_j - s_j\right)\right) + a_{i0}(t)(p_i - s_i - p_0)\right) \\
& - k_2 s_{\gamma_1}^{\alpha_2}\left(\sum_{j=1}^{n} a_{ij}(t)(v_i - v_j) + a_{i0}(t)(v_i - v_0)\right) + s_{\gamma_2}^{1}\left(\ddot{o}_{pi}\right)
\end{aligned} \tag{20}$$

For legitimate nodes $i \in \Lambda$, the tracking errors for the i-th followers are defined as

$$\begin{aligned}
\phi_{pi} &= \sum_{j\in N_i, j\in\Lambda} a_{ij}\left((p_i - s_i) - \left(p_j - s_j\right)\right) \\
\phi_{vi} &= \sum_{j\in N_i, j\in\Lambda} a_{ij}(v_i - v_j)
\end{aligned} \tag{21}$$

Define $\Phi_p = \left(\phi_{p1}^T, \phi_{p2}^T, \cdots, \phi_{pn_\Lambda}^T\right), \Phi_v = \left(\phi_{v1}^T, \phi_{v2}^T, \cdots, \phi_{vn_\Lambda}^T\right), n_\Lambda = card(\Lambda)$, consider the following Lyapunov function candidate

$$V_2(t) = k_1 \sum_{i=1}^{n_\Lambda} S_{\gamma_1}^{\alpha_1}\left(\phi_{pi}\right) + \frac{1}{2}\Phi_v^T\left((L+H)_\Lambda{}^{-1} \otimes I_3\right)\Phi_v \tag{22}$$

It follows from $a_{ij}(t) \geq a_{\min}$ that $V_2(t) \geq 0$, with equality holding if and only if $e = 0$. Now, consider the case when $t < T_1$, during which $\|\ddot{o}_{i0} - u_0\| \neq 0$. Due to the physical structure, it is clear that $\dot{V}_2(t) = k_1 \sum_{i=1}^{n_\Lambda} \dot{\phi}_{pi}^T s_{\gamma_1}^{\alpha_1}\left(\phi_{pi}\right) + \frac{1}{2}\Phi_v^T\left(\frac{d}{dt}(L+H)_\Lambda{}^{-1} \otimes I_m\right)\Phi_v + \Phi_v^T\left((L+H)_\Lambda{}^{-1} \otimes I_m\right)\dot{\Phi}_v$ is bounded. When $t > T_1$, we can get $o_{i0} = p_0$. Based on (21), we obtain the following error system.

$$\begin{aligned}
\dot{\phi}_{pi} =& \phi_{vi} \\
\dot{\phi}_{vi} =& -k_1\left(\sum_{j=1}^{n_\Lambda} a_{ij}\left(s_{\gamma_1}^{\alpha_1}\left(\phi_{pi}\right) - s_{\gamma_1}^{\alpha_1}\left(\phi_{pj}\right)\right) + a_{i0}s_{\gamma_1}^{\alpha_1}\left(\phi_{pi}\right)\right) \\
& - k_2\left(\sum_{j=1}^{n_\Lambda} a_{ij}\left(s_{\gamma_1}^{\alpha_2}\left(\phi_{vi}\right) - s_{\gamma_1}^{\alpha_2}\left(\phi_{vj}\right)\right) + a_{i0}s_{\gamma_1}^{\alpha_2}\left(\phi_{vi}\right)\right)
\end{aligned} \tag{23}$$

When $t > T_{trust}$, we obtain that $|a_{ij}(t) - a_{ij}^*| \leq \frac{M_\beta \varepsilon_d}{2(\lambda M_\beta + \bar{\Delta})}$. Hence, when $t > T_1 + T_{trust}$, we have

$$\begin{aligned}\dot{V}_2(t) =& k_1 \sum_{i=1}^{n_\Lambda} \dot{\phi}_{pi}^T s_{\gamma_1}^{\alpha_1}(\phi_{pi}) + \Phi_v^T \left((L+H)^{-1} \otimes I_m\right) \dot{\Phi}_v \\ =& k_1 \sum_{i=1}^{n_\Lambda} \phi_{vi}^T s_{\gamma_1}^{\alpha_1}(\phi_{pi}) + \sum_{i=1}^{n_\Lambda} \phi_{vi}^T \left(-k_1 s_{\gamma_1}^{\alpha_1}(\phi_{pi}) - k_2 s_{\gamma_1}^{\alpha_2}(\phi_{vi})\right) \\ =& k_1 \sum_{i=1}^{n_\Lambda} \phi_{vi}^T s_{\gamma_1}^{\alpha_1}(\phi_{pi}) - k_1 \sum_{i=1}^{n_\Lambda} \phi_{vi}^T s_{\gamma_1}^{\alpha_1}(\phi_{pi}) - k_2 \sum_{i=1}^{n_\Lambda} \phi_{vi}^T s_{\gamma_1}^{\alpha_2}(\phi_{vi}) \\ =& -k_2 \sum_{i=1}^{n_\Lambda} \phi_{vi}^T s_{\gamma_1}^{\alpha_2}(\phi_{vi})\end{aligned} \tag{24}$$

It follows from (14) that

$$-k_2 \sum_{i=1}^{n_\Lambda} \phi_{vi}^T s_{\gamma_1}^{\alpha_2}(\phi_{vi}) = \begin{cases} -k_2 \sum_{i=1}^{n_\Lambda} \sum_{l=1}^{3} \gamma_1^{\alpha_2} |\phi_{vil}|, |\phi_{vil}| > \gamma_1 \\ -k_2 \sum_{i=1}^{n_\Lambda} \sum_{l=1}^{3} |\phi_{vil}|^{\alpha_2+1}, |\phi_{vil}| \leq \gamma_1 \end{cases} \tag{25}$$

When $|\phi_{vil}| > \gamma_1$, we can obtain $\dot{V}_2(t) = -k_2 \sum_{i=1}^{n_\Lambda} \sum_{l=1}^{3} \gamma_1^{\alpha_2} |\phi_{vil}| < 0$. By Barbalat's lemma, $\dot{V}_2(t) \to 0$ as $t \to \infty$. When $0 < |\phi_{vil}| \leq \gamma_1$, we have $\dot{V}_2(t) = -k_2 \sum_{i=1}^{n_\Lambda} \sum_{l=1}^{3} |\phi_{vil}|^{\alpha_2+1} < 0$. Finally, from the algebraic structure of $\dot{V}_2(t)$, $\dot{V}_4(t) \to 0$ implies that ϕ_{vi} and subsequently ϕ_{pi} for all legitimate followers. Consequently, ϕ_{pi} and ϕ_{vi} will asymptotically converge to a neighborhood of zero.

It follows from (25) that $\dot{V}_2(t) \leq 0$. The non-positive definiteness of $\dot{V}_2(t) \leq 0$ implies the non-expansive property $V_2(t) \leq V_2(0), \quad \forall t \geq 0$, which guarantees uniform boundedness of the tracking errors $\{\phi_{pi}, \phi_{vi}\}$ for all $t > 0$. Due to the uncertainty of the initial state, which may satisfy either $|\phi_{pil}| > \gamma_1, |\phi_{vil}| > \gamma_1$ or $|\phi_{pil}| \leq \gamma_1, |\phi_{vil}| \leq \gamma_1$, the maximum settling time is estimated by assuming $|\phi_{pil}| > \gamma_1, |\phi_{vil}| > \gamma_1$. Under the condition $|\phi_{pil}| > \gamma_1, |\phi_{vil}| > \gamma_1, \quad (i,l) \in \{1, \ldots, n\} \times \{1, \ldots, m\}$, we subsequently establish the finite-time convergence $\limsup_{t \to T} |\phi_{pil}(t)| < \gamma_1 \quad \text{and} \quad \limsup_{t \to T} |\phi_{vil}(t)| < \gamma_1$, where $T < \infty$ denotes the convergence time horizon. This convergence property permits the error dynamics transformation:

$$\begin{aligned}\dot{\phi}_{pi} =& \phi_{vi} \\ \dot{\phi}_{vi} =& -k_1 \left(\sum_{j=1}^{n_\Lambda} a_{ij} \gamma_1^{\alpha_1} (\mathrm{sgn}(\phi_{pi}) - \mathrm{sgn}(\phi_{pj})) + a_{i0} \gamma_1^{\alpha_1} \mathrm{sgn}(\phi_{pi}) \right) \\ & - k_2 \left(\sum_{j=1}^{n_\Lambda} a_{ij} \gamma_1^{\alpha_1} (\mathrm{sgn}(\phi_{vi}) - \mathrm{sgn}(\phi_{vj})) + a_{i0} \gamma_1^{\alpha_1} \mathrm{sgn}(\phi_{vi}) \right)\end{aligned} \tag{26}$$

We can conclude that system (26) is homogeneous. Lemma 1 consequently establishes the local finite-time stability property for (26). Specifically, (26) has a degree of $k = -1$ with respect to the vector $(2,2,2,1,1,1)$. The time derivative of the Lyapunov function satisfies $\dot{V}_2(t) = -k_2 \sum_{i=1}^{n_\Lambda} \sum_{l=1}^{3} \gamma_1^{\alpha_2} |\phi_{vil}| < 0, \quad \forall |\phi_{vil}| \geq \gamma_1$, which rigorously proves global asymptotic stability. Furthermore, the tracking errors exhibit finite-time convergence $\exists T < \infty : \phi_{pi}(t) = 0_m, \phi_{vi}(t) = 0_m, \quad \forall t \geq T$.

The ultimate boundedness property guarantees $\begin{cases} |\phi_{pil}(t)| < \gamma_1 \\ |\phi_{vil}(t)| < \gamma_1 \end{cases}, \quad \forall t \geq T, (i,l) \in \{1,\ldots,N\} \times \{1,2,3\}$, where the errors remain permanently within the γ_1-neighborhood. When $|\phi_{pil}| \leq \gamma_1, |\phi_{vil}| \leq \gamma_1$, the error system (23) becomes

$$\begin{aligned}\dot{\phi}_{pi} =& \phi_{vi}\\ \dot{\phi}_{vi} =& -k_1\left(\sum_{j=1}^{n_\Lambda} a_{ij}\left(sig\left(\phi_{pi}\right)^{\alpha_1} - sig\left(\phi_{pj}\right)^{\alpha_1}\right) + a_{i0}sig\left(\phi_{pi}\right)^{\alpha_1}\right)\\ & -k_2\left(\sum_{j=1}^{n_\Lambda} a_{ij}\left(sig(\phi_{vi})^{\alpha_2} - sig\left(\phi_{vj}\right)^{\alpha_2}\right) + a_{i0}sig(\phi_{vi})^{\alpha_2}\right)\end{aligned} \tag{27}$$

We can conclude that system (27) is homogeneous. Lemma 1 consequently establishes the local finite-time stability property for (27). Specifically, (27) has a degree of $k = \alpha_2 - 1$ with respect to the vector $\left(\frac{1}{1+\alpha_1}, \frac{1}{1+\alpha_1}, \frac{1}{1+\alpha_1}, 1, 1, 1\right)$. The time derivative satisfies $\dot{V}_2(t) = -k_2 \sum_{i=1}^{n}\sum_{l=1}^{m} |\phi_{vil}|^{\alpha_2+1} < 0, 0 < |\phi_{vil}| \le \gamma_1$, which implies that ϕ_{pi} and ϕ_{vi} will asymptotically converge to a neighborhood of zero.

In order to estimate the maximum settling time, the initial state is assumed to satisfy $|\phi_{pil}| > \gamma_1, |\phi_{vil}| > \gamma_1$, under which the error system is defined as (26). A new Lyapunov function is defined to evaluate the settling time

$$V_3(t) = V_2^{\frac{3}{2}}(t) + \rho\Phi_p^T\left((L+H)_\Lambda{}^{-1} \otimes I_3\right)\Phi_v, \rho > 0 \tag{28}$$

By applying Lemma 2, one can obtain that

$$\begin{aligned}\rho\Phi_p^T\left((L+H)^{-1} \otimes I_3\right)\Phi_v \ge& -\rho\left\|\Phi_p\right\|\left\|(L+H)^{-1}\right\|\|\Phi_v\|\\ \ge& -\frac{2\rho}{3\lambda_{\min}}c^{\frac{3}{2}}\left\|\Phi_p\right\|^{\frac{3}{2}} - \frac{\rho}{3\lambda_{\min}}c^{-3}\|\Phi_v\|^3\end{aligned} \tag{29}$$

$$\begin{aligned}V_2^{\frac{3}{2}}(t) =& \left(k_1\sum_{i=1}^{n_\Lambda} S_{\gamma_1}^{\alpha_1}\left(\phi_{pi}\right) + \frac{1}{2}\Phi_v^T\left((L+H)^{-1} \otimes I_3\right)\Phi_v\right)^{\frac{3}{2}}\\ \ge& k_1^{\frac{3}{2}}\sum_{i=1}^{n_\Lambda}\sum_{l=1}^{3}\left(\frac{\gamma_1^{\alpha_1}}{\alpha_1+1}|\phi_{pi}|\right)^{\frac{3}{2}} + \left(\frac{1}{2\lambda_{\max}}\right)^{\frac{3}{2}}\|\Phi_v\|^3\\ \ge& \left(\frac{k_1\gamma_1^{\alpha_1}}{\alpha_1+1}\right)^{\frac{3}{2}}\left\|\Phi_p\right\|^{\frac{3}{2}} + \left(\frac{1}{2\lambda_{\max}}\right)^{\frac{3}{2}}\|\Phi_v\|^3\end{aligned} \tag{30}$$

where c is a positive constant, $\lambda_{\min}, \lambda_{\max}$ denote the minimum and maximum eigenvalues of $(L+H)_\Lambda$, respectively. Combining (3) and (4) yields:

$$V_3(t) \ge \left(\left(\frac{k_1\gamma_1^{\alpha_1}}{\alpha_1+1}\right)^{\frac{3}{2}} - \frac{2\rho}{3\lambda_{\min}}c^{\frac{3}{2}}\right)\left\|\Phi_p\right\|^{\frac{3}{2}} + \left(\left(\frac{1}{2\lambda_{\max}}\right)^{\frac{3}{2}} - \frac{\rho}{3\lambda_{\min}}c^{-3}\right)\|\Phi_v\|^3 \tag{31}$$

An appropriate selection of the parameter c, subject to the satisfaction of condition $\sqrt{2\lambda_{\max}}^3\sqrt{\frac{\rho}{3\lambda_{\min}}} < c < \frac{k_1\gamma_1^{\alpha_1}}{\alpha_1+1}\left(\frac{3\lambda_{\min}}{2\rho}\right)^{\frac{2}{3}}$, guarantees the positivity of the coefficients $\left(\frac{k_1\gamma_1^{\alpha_1}}{\alpha_1+1}\right)^{\frac{3}{2}} - \frac{2\rho}{3\lambda_{\min}}c^{\frac{3}{2}}$ and $\left(\frac{1}{2\lambda_{\max}}\right)^{\frac{3}{2}} - \frac{\rho}{3\lambda_{\min}}c^{-3}$ in Equation (31). Similarly, we can obtain

$$\rho\Phi_p^T\left((L+H)^{-1} \otimes I_3\right)\Phi_v \le \frac{\rho}{\lambda_{\min}}\left\|\Phi_p\right\|\|\Phi_v\| \le \frac{\rho}{\lambda_{\min}}\left(\frac{2}{3}c^{\frac{2}{3}}\left\|\Phi_p\right\|^{\frac{3}{2}} + \frac{1}{3c^3}\|\Phi_x\|^3\right) \tag{32}$$

$$\begin{aligned}V_2^{\frac{3}{2}}(t) =& \left(k_1\sum_{i=1}^{n_\Lambda} S_{\gamma_1}^{\alpha_1}\left(\phi_{pi}\right) + \frac{1}{2}\Phi_v^T\left((L+H)^{-1} \otimes I_3\right)\Phi_v\right)^{\frac{3}{2}}\\ \le& \sqrt{2}\left(\left(k_1\sum_{i=1}^{n_\Lambda} S_{\gamma_1}^{\alpha_1}\left(\phi_{pi}\right)\right)^{\frac{3}{2}} + \left(\frac{1}{2}\Phi_v^T\left((L+H)^{-1} \otimes I_3\right)\Phi_v\right)^{\frac{3}{2}}\right)\\ \le& \sqrt{2}\left(\frac{k_1\gamma_1^{\alpha_1}(2\alpha_1+1)\sqrt{3n}}{\alpha_1+1}\right)^{\frac{3}{2}}\left\|\Phi_p\right\|^{\frac{3}{2}} + \left(\frac{1}{2\lambda_{\min}}\right)^{\frac{3}{2}}\|\Phi_v\|^3\end{aligned} \tag{33}$$

Consequently, we obtain the following expression

$$\begin{aligned} V_3(t) \le & \left(\sqrt{2}\left(\frac{k_1\gamma_1^{\alpha_1}(2\alpha_1+1)\sqrt{3n}}{\alpha_1+1} \right)^{\frac{3}{2}} + \frac{2}{3}\frac{\rho}{\lambda_{\min}}c^{\frac{2}{3}} \right) \left\|\Phi_p\right\|^{\frac{3}{2}} + \left(\frac{1}{2\lambda_{\min}} + \frac{1}{3c^3}\frac{\rho}{\lambda_{\min}} \right)^{\frac{3}{2}} \|\Phi_v\|^3 \\ = & \varpi_1 \left\|\Phi_p\right\|^{\frac{3}{2}} + \varpi_2 \|\Phi_v\|^3 \end{aligned} \tag{34}$$

where $\varpi_1 = \sqrt{2}\left(\frac{k_1\gamma_1^{\alpha_1}(2\alpha_1+1)\sqrt{3n}}{\alpha_1+1} \right)^{\frac{3}{2}} + \frac{2}{3}\frac{\rho}{\lambda_{\min}}c^{\frac{2}{3}}$ and $\varpi_2 = \left(\frac{1}{2\lambda_{\min}} + \frac{1}{3c^3}\frac{\rho}{\lambda_{\min}} \right)^{\frac{3}{2}}$.

Taking the time derivative of the constructed Lyapunov function $V_3(t)$ yields

$$\begin{aligned} \dot{V}_3(t) \le & -\frac{3k_2\gamma_1^{\alpha_1}}{2}\sqrt{\frac{1}{2\lambda_{\min}}}\|\Phi_v\|^2 + \frac{\rho}{\lambda_{\min}}\|\Phi_v\|^2 - k_1\rho\gamma_1^{\alpha_1}\left\|\Phi_p\right\| + k_2\rho\sqrt{3n}\gamma_1^{\alpha_2}\left\|\Phi_p\right\| \\ = & -\left(\frac{3k_2\gamma_1^{\alpha_1}}{2}\sqrt{\frac{1}{2\lambda_{\min}}} - \frac{\rho}{\lambda_{\min}} \right)\|\Phi_v\|^2 - \left(k_1\rho\gamma_1^{\alpha_1} - k_2\rho\sqrt{3n}\gamma_1^{\alpha_2} \right)\left\|\Phi_p\right\| \\ \le & -\left[\left(\frac{3k_2\gamma_1^{\alpha_1}}{2}\sqrt{\frac{1}{2\lambda_{\min}}} - \frac{\rho}{\lambda_{\min}} \right)^{\frac{3}{2}}\|\Phi_v\|^3 + \left(k_1\rho\gamma_1^{\alpha_1} - k_2\rho\sqrt{3n}\gamma_1^{\alpha_2} \right)^{\frac{3}{2}}\left\|\Phi_p\right\|^{\frac{3}{2}} \right]^{\frac{2}{3}} \\ \le & -\varpi V_3(t)^{\frac{2}{3}} \end{aligned} \tag{35}$$

where $\varpi = \min\left\{ \frac{\frac{3k_2\gamma_1^{\alpha_1}}{2}\sqrt{\frac{1}{2\lambda_{\min}}} - \frac{\rho}{\lambda_{\min}}}{\varpi_1^{\frac{2}{3}}}, \frac{k_1\rho\gamma_1^{\alpha_1} - k_2\rho\sqrt{3n}\gamma_1^{\alpha_2}}{\varpi_2^{\frac{2}{3}}} \right\}$.

Lemma 1 implies that system (26) achieves finite-time stability within $T_2 \le \frac{3\sqrt[3]{V_3(0)}}{\varpi}$. From the definition (21), we can obtain that $\left\|\Phi_p\right\| = \left\|((L+H)_\Lambda \otimes I_m)(p_\Lambda - I_{n_\Lambda}p_0)\right\| = 0$ and $\|\Phi_v\| = \left\|((L+H)_\Lambda \otimes I_m)(v_\Lambda - I_{n_\Lambda}v_0)\right\| = 0$, when $\forall t \ge T_{trust} + T_1 + T_2$. Obviously, $(L+H)_\Lambda$ is positive definite and symmetric, we further get $p_i = p_0$ and $v_i = v_0$, when $\forall t \ge T_{trust} + T_1 + T_2$. Consequently, the closed-loop formation system (1)(2) is stabilized in finite time by using the control algorithm (17). This completes the proof. □

3.3. Fixed-Time Formation Control Subject to Sybil Attacks and Input Saturation

Next, we investigate the fixed-time formation tracking problem for systems (1) and (2) in the presence of Sybil attacks and input saturation. By incorporating a dynamic trust-accumulating adjacency weight and a hyperbolic tangent function [38], we design the control input (36) to achieve fixed-time formation tracking.

$$\begin{pmatrix} \eta_{xi}(t) \\ \eta_{yi}(t) \\ \eta_{zi}(t) \end{pmatrix} = \frac{1}{g}\begin{bmatrix} \cos\theta_i\cos\psi_i & \sin\theta_i & -\cos\theta_i\sin\psi_i \\ -\sin\theta_i\cos\psi_i & \cos\theta_i & 0 \\ \sin\psi_i & 0 & \cos\psi_i \end{bmatrix}\begin{pmatrix} \dot{v}_{xi} \\ \dot{v}_{yi} + g \\ \dot{v}_{zi} \end{pmatrix}$$

$$\begin{aligned} \begin{pmatrix} \dot{v}_{xi} \\ \dot{v}_{yi} \\ \dot{v}_{zi} \end{pmatrix} = & -\frac{h_1}{n+1}\left(\sum_{j=1}^{n} a_{ij}\tanh sig^{\alpha_1}\left((p_i - s_i) - \left(p_j - s_j \right) \right) + a_{i0}\tanh sig^{\alpha_1}(p_i - s_i - p_0) \right) \\ & -\frac{h_2}{n+1}\left(\sum_{j=1}^{n} a_{ij}\tanh sig^{\alpha_2}(v_i - v_j) + a_{i0}\tanh sig^{\alpha_2}(v_i - v_0) \right) \\ & -\frac{h'_1}{n+1}\left(\sum_{j=1}^{n} a_{ij}\tanh sig^{\tilde{\alpha}_1}\left((p_i - s_i) - \left(p_j - s_j \right) \right) + a_{i0}\tanh sig^{\tilde{\alpha}_1}(p_i - s_i - p_0) \right) \\ & -\frac{h'_2}{n+1}\left(\sum_{j=1}^{n} a_{ij}\tanh sig^{\tilde{\alpha}_2}(v_i - v_j) + a_{i0}\tanh sig^{\tilde{\alpha}_2}(v_i - v_0) \right) + s^1_{\gamma_2}\left(\ddot{o}_{pi} \right) \end{aligned} \tag{36}$$

where $tanh(\bullet)$ denotes hyperbolic tangent function, weight $a_{ij}(t)$ is governed by (6), $h_1 = diag\left\{h_{1x}, h_{1y}, h_{1z}\right\} > 0, h'_1 = diag\left\{h'_{1x}, h'_{1y}, h'_{1z}\right\} > 0, h_2 = diag\left\{h_{2x}, h_{2y}, h_{2z}\right\} > 0, h'_2 =$

$diag\{h'_{2x}, h'_{2y}, h'_{2z}\} > 0$ denote the gain coefficients, $\alpha_1 = \frac{\alpha_2}{2-\alpha_2}, \alpha_2 \in (0,1), \tilde{\alpha}_1 = \frac{4-3\alpha_2}{2-\alpha_2}, \tilde{\alpha}_2 = \frac{4-3\alpha_2}{3-2\alpha_2}, s^1_{\gamma_2}(p) = \left(s^1_{\gamma_{x2}}(p_x), s^1_{\gamma_{y2}}(p_y), s^1_{\gamma_{z2}}(p_z)\right)^T, \gamma_{x2}, \gamma_{y2}, \gamma_{z2} > 0.$

Theorem 3. *Consider a networked system (1) (2) containing n follower UAVs subject to input saturation and Sybil attacks, and a leader UAV . Under Assumption 1, the fixed-time control algorithm (36) is developed by employing the confidence weight (6), and hyperbolic tangent function. Choose* $h_1, h'_1, h_2, h'_2 > 0$, $\alpha_1 = \frac{\alpha_2}{2-\alpha_2}, \alpha_2 \in (0,1), \tilde{\alpha}_1 = \frac{4-3\alpha_2}{2-\alpha_2}, \tilde{\alpha}_2 = \frac{4-3\alpha_2}{3-2\alpha_2}$. *Then, there exists a neighborhood D of the origin such that, for any initial condition with* $e \in D$, *the tracking errors* $e_i = \begin{bmatrix} e_{1i}^T & e_{2i}^T \end{bmatrix}^T$ *satisfy* $e \in D$ *and the trajectories reach the origin within a fixed time* $t \le T_{trust} + T_1 + T_2$, *where*

$$D = \begin{cases} \mathbb{R}^{6n_\Lambda}, r < 1 \\ \left\{ e \middle| V(e) \le k^\eta \left(\frac{\frac{|\lambda|\chi^{\eta-1}}{2m} - \sqrt{\left(\frac{|\lambda|\chi^{\eta-1}}{2m}\right)^2 - 4\varepsilon_1\varepsilon_2\alpha_l\beta_l}}{2\varepsilon_2\alpha_l\beta_l} \right)^\eta \right\}, r \ge 1 \end{cases}$$

$$T_2 \le \begin{cases} \frac{\eta}{\varepsilon_2\alpha_l\beta_l k_1}\left(\frac{\pi}{2} - \tan^{-1}k_2\right), r < 1 \\ \frac{\eta k}{(1-k)\sqrt{\varepsilon_1\varepsilon_2\alpha_l\beta_l}}, r \ge 1 \end{cases}$$

where the parameters are defined in (54) and (55).

Furthermore, h_1, h'_1, h_2, h'_2 *should be chosen in accordance with the actuator's saturation limit to ensure operational feasibility, i.e.,*

$$\begin{cases} |\dot{v}_{xi}| \le \gamma_{x2} + \frac{\sum_{j=0}^{n} a_{ij}}{n+1}(h_{1x} + h_{2x} + h'_{1x} + h'_{2x}) \le \frac{g}{\sqrt{3}}\eta_{\min} \\ \left|\dot{v}_{yi} + g\right| \le \gamma_{y2} + \frac{\sum_{j=0}^{n} a_{ij}}{n+1}\left(h_{1y} + h_{2y} + h'_{1y} + h'_{2y}\right) + g \le \frac{g}{\sqrt{3}}\eta_{\min} \\ |\dot{v}_{zi}| \le \gamma_{z2} + \frac{\sum_{j=0}^{n} a_{ij}}{n+1}(h_{1z} + h_{2z} + h'_{1z} + h'_{2z}) \le \frac{g}{\sqrt{3}}\eta_{\min} \end{cases} \tag{37}$$

Proof. The inequality in (37) is a sufficient condition to ensure that the attitude-independent acceleration commands generated by the fixed-time controller (36) remain within the conservative bounds given in (19). In particular, using the fact that $a_{ij}(t)$ are generated by (6), we have $0 < a_{ij}(t) \le a_{\max}$ for all $t \ge 0$. Combined with the uniform boundedness of the hyperbolic tangent terms $|\tanh(\cdot)| \le 1$, $\sum_{j=0}^{n} a_{ij} \Big/ (n+1) \le 1$, (37) provides an upper bound on $|\dot{v}_{xi}(t)|$, $|\dot{v}_{yi}(t) + g|$, and $|\dot{v}_{zi}(t)|$. Consequently, by the construction of (19), the corresponding overload components $\eta_{xi}(t), \eta_{yi}(t), \eta_{zi}(t)$ computed through the rotation-based mapping in (16) satisfy the actuator constraints. Clearly, the magnitude of the control input (36) depends only on the parameters $\gamma_2, h_1, h_2, h'_1, h'_2, a_{max}$. Therefore, the control input designed using the hyperbolic tangent function is inherently bounded, ensuring that it does not exceed the physical actuation limit of the UAVs.

Next, we will show that the states of all legitimate follower UAVs can track that of the leader in a practical fixed-time.

Step 1. Global Asymptotical Stability: For legitimate nodes $i \in \Lambda$, by defining the tracking errors $e_{1i} = p_i - s_i - p_0, e_{2i} = v_i - v_0$, consider the following Lyapunov function

$$\begin{aligned} V_4(t) =& \frac{h_1}{n_\Lambda+1}\sum_{i=1}^{n_\Lambda}\sum_{j=1}^{n_\Lambda}\sum_{l=1}^{3}a_{ij}\int_0^{e_{1il}-e_{1jl}}\tanh(sig^{\alpha_1}(s))ds + \frac{2h_1}{n_\Lambda+1}\sum_{i=1}^{n_\Lambda}\sum_{l=1}^{3}a_{i0}\int_0^{e_{1il}}\tanh(sig^{\alpha_1}(s))ds \\ &+ \frac{h'_1}{n_\Lambda+1}\sum_{i=1}^{n_\Lambda}\sum_{j=1}^{n_\Lambda}\sum_{l=1}^{3}a_{ij}\int_0^{e_{1il}-e_{1jl}}\tanh\left(sig^{\tilde{\alpha}_1}(s)\right)ds \\ &+ \frac{2h'_1}{n_\Lambda+1}\sum_{i=1}^{n_\Lambda}\sum_{l=1}^{3}a_{i0}\int_0^{e_{1il}}\tanh\left(sig^{\tilde{\alpha}_1}(s)\right)ds + e_2^Te_2 \end{aligned} \tag{38}$$

where $e_2 = \left(e_{21}^T, e_{22}^T, \cdots, e_{2n_\Lambda}^T\right)^T$. Since for any $e \neq 0$, the inequality $a_{ij}(t) \geq a_{\min}$, $\int_0^e \tanh(sig^\alpha(s))ds > 0$ hold, it follows that $V_4(t)$ is valid. Similar to Theorem 2, consider the case when $t < T_1$, during which $\dot{V}_4$ is bounded. When $t > T_1$, we can get $\ddot{o}_{pi} = \ddot{p}_0$. When $t > T_{trust}$, we obtain that $|a_{ij}(t) - a_{ij}^*| \leq \frac{M_\beta \varepsilon_d}{2\left(\lambda M_\beta + \tilde{\Delta}\right)}$. Hence, when $t > T_1 + T_{trust}$, we have

$$\begin{aligned} \dot{V}_4(t) =& \frac{h_1}{n_\Lambda+1}\sum_{i=1}^{n_\Lambda}\sum_{j=1}^{n_\Lambda}\sum_{l=1}^{3}a_{ij}\tanh\left(sig^{\alpha_1}\left(e_{1il}-e_{1jl}\right)\right)\left(e_{2il}-e_{2jl}\right) + \frac{2h_1}{n_\Lambda+1}\sum_{i=1}^{n_\Lambda}\sum_{l=1}^{3}a_{i0}\tanh(sig^{\alpha_1}(e_{1il}))e_{2il} \\ &+ \frac{h'_1}{n_\Lambda+1}\sum_{i=1}^{n_\Lambda}\sum_{j=1}^{n_\Lambda}\sum_{l=1}^{3}a_{ij}\tanh\left(sig^{\tilde{\alpha}_1}\left(e_{1il}-e_{1jl}\right)\right)\left(e_{2il}-e_{2jl}\right) \\ &+ \frac{2h'_1}{n_\Lambda+1}\sum_{i=1}^{n_\Lambda}\sum_{l=1}^{3}a_{i0}\tanh\left(sig^{\tilde{\alpha}_1}(e_{1il})\right)e_{2il} + 2e_2^T\left(\dot{v}_i - 1_n\otimes\ddot{o}_{pi}\right) \end{aligned} \tag{39}$$

where $v = \left(v_1^T, v_2^T, \cdots, v_{n_\Lambda}^T\right)^T$. The formation tracking system (1) (2) with control algorithm (36) can be rewritten as

$$\begin{aligned} \dot{e}_{1i} =& e_{2i} \\ \dot{e}_{2i} =& -\frac{h_1}{n_\Lambda+1}\left(\sum_{j=1}^{n_\Lambda}a_{ij}\tanh sig^{\alpha_1}\left(e_{1i}-e_{1j}\right) + a_{i0}\tanh sig^{\alpha_1}(e_{1i})\right) \\ &-\frac{h_2}{n_\Lambda+1}\left(\sum_{j=1}^{n_\Lambda}a_{ij}\tanh sig^{\alpha_2}\left(e_{2i}-e_{2j}\right) + a_{i0}\tanh sig^{\alpha_2}(e_{2i})\right) \\ &-\frac{h'_1}{n_\Lambda+1}\left(\sum_{j=1}^{n_\Lambda}a_{ij}\tanh sig^{\tilde{\alpha}_1}\left(e_{1i}-e_{1j}\right) + a_{i0}\tanh sig^{\tilde{\alpha}_1}(e_{1i})\right) \\ &-\frac{h'_2}{n_\Lambda+1}\left(\sum_{j=1}^{n_\Lambda}a_{ij}\tanh sig^{\tilde{\alpha}_2}\left(e_{2i}-e_{2j}\right) + a_{i0}\tanh sig^{\tilde{\alpha}_2}(e_{2i})\right) \end{aligned} \tag{40}$$

Substituting equation (40) into equation (39) yields:

$$\begin{aligned} \dot{V}_4(t) =& -\frac{h_2}{n_\Lambda+1}\sum_{i=1}^{n_\Lambda}\sum_{j=1}^{n_\Lambda}\sum_{l=1}^{3}a_{ij}\tanh\left(sig^{\alpha_2}\left(e_{2il}-e_{2jl}\right)\right)\left(e_{2il}-e_{2jl}\right) \\ &-\frac{2h_2}{n_\Lambda+1}\sum_{i=1}^{n_\Lambda}\sum_{l=1}^{3}a_{i0}\tanh(sig^{\alpha_2}(e_{2il}))e_{2il} \\ &-\frac{h'_2}{n_\Lambda+1}\sum_{i=1}^{n_\Lambda}\sum_{j=1}^{n_\Lambda}\sum_{l=1}^{3}a_{ij}\tanh\left(sig^{\tilde{\alpha}_2}\left(e_{2il}-e_{2jl}\right)\right)\left(e_{2il}-e_{2jl}\right) \\ &-\frac{2h'_2}{n_\Lambda+1}\sum_{i=1}^{n_\Lambda}\sum_{l=1}^{3}a_{i0}\tanh\left(sig^{\tilde{\alpha}_2}(e_{2il})\right)e_{2il} \end{aligned} \tag{41}$$

By Barbalat's lemma, $\dot{V}_4(t) \to 0$ as $t \to \infty$. Finally, from the algebraic structure of $\dot{V}_4(t)$, $\dot{V}_4(t) \to 0$ implies $e_{2i}(t) \to 0$ and subsequently $e_{1i}(t) \to 0$ for all legitimate followers. Hence $e(t) \to 0$ as $t \to \infty$.

Step 2. Local Fixed-Time Stability: In this step, we prove that system (40) is fixed-time stable. According to [38], the hyperbolic tangent function can be expanded as $\tanh(sig^{\alpha}(x)) = sig^{\alpha}(x) + o(sig^{\alpha}(x))$. The system (40) can be rewritten as

$$\begin{cases} \dot{e}_{1i} = e_{2i} \\ \dot{e}_{2i} = \hbar_{i\ell}(e_{1i}, e_{2i}) + \hbar_{iv}(e_{1i}, e_{2i}) + \tilde{\hbar}_i(e_{1i}, e_{2i}) \end{cases} \tag{42}$$

where

$$\begin{aligned} \hbar_{i\ell}(e_{1i}, e_{2i}) = &-\frac{h_1}{n_\Lambda + 1}\left(\sum_{j=1}^{n_\Lambda} a_{ij} sig^{\alpha_1}\left(e_{1i} - e_{1j}\right) + a_{i0} sig^{\alpha_1}(e_{1i})\right) \\ &-\frac{h_2}{n_\Lambda + 1}\left(\sum_{j=1}^{n_\Lambda} a_{ij} sig^{\alpha_2}\left(e_{2i} - e_{2j}\right) + a_{i0} sig^{\alpha_2}(e_{2i})\right) \\ \hbar_{iv}(e_{1i}, e_{2i}) = &-\frac{h'_1}{n_\Lambda + 1}\left(\sum_{j=1}^{n_\Lambda} a_{ij} sig^{\tilde{\alpha}_1}\left(e_{1i} - e_{1j}\right) + a_{i0} sig^{\tilde{\alpha}_1}(e_{1i})\right) \\ &-\frac{h'_2}{n_\Lambda + 1}\left(\sum_{j=1}^{n_\Lambda} a_{ij} sig^{\tilde{\alpha}_2}\left(e_{2i} - e_{2j}\right) + a_{i0} sig^{\tilde{\alpha}_2}(e_{2i})\right) \\ \tilde{\hbar}_i(e_{1i}, e_{2i}) = &-\frac{h_1}{n_\Lambda + 1}\left(\sum_{j=1}^{n_\Lambda} a_{ij} o\left(sig^{\alpha_1}\left(e_{1i} - e_{1j}\right)\right) + a_{i0} o(sig^{\alpha_1}(e_{1i}))\right) \\ &-\frac{h_2}{n_\Lambda + 1}\left(\sum_{j=1}^{n_\Lambda} a_{ij} o\left(sig^{\alpha_2}\left(e_{2i} - e_{2j}\right)\right) + a_{i0} o(sig^{\alpha_2}(e_{2i}))\right) \\ &-\frac{h'_1}{n_\Lambda + 1}\left(\sum_{j=1}^{n_\Lambda} a_{ij} o\left(sig^{\tilde{\alpha}_1}\left(e_{1i} - e_{1j}\right)\right) + a_{i0} o(sig^{\tilde{\alpha}_1}(e_{1i}))\right) \\ &-\frac{h'_2}{n_\Lambda + 1}\left(\sum_{j=1}^{n_\Lambda} a_{ij} o\left(sig^{\tilde{\alpha}_2}\left(e_{2i} - e_{2j}\right)\right) + a_{i0} o(sig^{\tilde{\alpha}_2}(e_{2i}))\right) \end{aligned}$$

By Definition 1, it can be obtained that the system

$$\begin{cases} \dot{e}_{1i} = e_{2i} \\ \dot{e}_{2i} = \hbar_{i\ell}(e_{1i}, e_{2i}) \end{cases} \tag{43}$$

is a homogeneous system with respect to the vector $r_\ell = (r_{\ell 1}, r_{\ell 1}, r_{\ell 1}, r_{\ell 2}, r_{\ell 2}, r_{\ell 2})$, with a homogeneity degree of $k_0 = -1 < 0$, $r_{\ell 1} = \frac{2-\alpha_2}{1-\alpha_2}, r_{\ell 2} = \frac{1}{1-\alpha_2}$.

Consider the following new Lyapunov function

$$V_\ell(t) = \frac{h_1}{n_\Lambda + 1}\sum_{i=1}^{n_\Lambda}\left(\sum_{j=1}^{n_\Lambda}\sum_{l=1}^{3} a_{ij}\left|e_{1il} - e_{1jl}\right|^{1+\alpha_1} + 2a_{i0}|e_{1il}|^{1+\alpha_1}\right) + \sum_{i=1}^{n_\Lambda}\sum_{l=1}^{3}|e_{2il}|^2 \tag{44}$$

Taking the time derivative of the Lyapunov function $V_\ell(t)$ yields:

$$\dot{V}_\ell(t) = -\frac{h_2}{n_\Lambda + 1}\sum_{i=1}^{n_\Lambda}\left(\sum_{j=1}^{n_\Lambda}\sum_{l=1}^{3} a_{ij}\left|e_{2il} - e_{2jl}\right|^{1+\alpha_2} + 2a_{i0}|e_{2il}|^{1+\alpha_2}\right) \le 0 \tag{45}$$

It follows from (45) that system (43) is globally asymptotically stable. Similarity, one can obtain that the system

$$\begin{cases} \dot{e}_{1i} = e_{2i} \\ \dot{e}_{2i} = \hbar_{iv}(e_{1i}, e_{2i}) \end{cases} \tag{46}$$

is a homogeneous system with respect to the vector $r_v = (r_{v1}, r_{v1}, r_{v1}, r_{v2}, r_{v2}, r_{v2})$, with a homogeneity degree of $k_\infty = 1 > 0$, $r_{v1} = \frac{2-\alpha_2}{1-\alpha_2}, r_{v2} = \frac{3-2\alpha_2}{1-\alpha_2}$. Consider a Lyapunov function $V_v(t) = \frac{h'_1}{n_\Lambda+1}\sum_{i=1}^{n_\Lambda}\left(\sum_{j=1}^{n_\Lambda}\sum_{l=1}^{3} a_{ij}\left|e_{1il} - e_{1jl}\right|^{1+\tilde{\alpha}_1} + 2a_{i0}|e_{1il}|^{1+\tilde{\alpha}_1}\right) + \sum_{i=1}^{n_\Lambda}\sum_{l=1}^{3}|e_{2il}|^2$. Its derivative

satisfies $\dot{V}_v(t) = -\frac{h'_2}{n_\Lambda+1}\sum_{i=1}^{n_\Lambda}\left(\sum_{j=1}^{n_\Lambda}\sum_{l=1}^{3}a_{ij}\left|e_{2il}-e_{2jl}\right|^{1+\tilde{\alpha}_2}+2a_{i0}|e_{2il}|^{1+\tilde{\alpha}_2}\right)\le 0$. This ensures the global asymptotic stability of system (46).

According to Lemma 4, for the negative degree $k_0 = -1$ and weights $r_{\ell 1}$ and $r_{\ell 2}$, substituting a sufficiently small χ into the following limits yields $\lim_{\chi\to 0}\frac{\tilde{h}_i(\chi^{r_{\ell 1}}e_{1i},\chi^{r_{\ell 2}}e_{2i})}{\chi^{k_0+r_{\ell 1}}} = 0, \lim_{\chi\to 0}\frac{\tilde{h}_i(\chi^{r_{\ell 1}}e_{1i},\chi^{r_{\ell 2}}e_{2i})}{\chi^{k_0+r_{\ell 2}}} = 0$. According to Lemma 4, the system (42) is local fixed-time stable. Hence, it can be concluded that the formation tracking control is fixed-time stable.

Finally, practical fixed-time stability: Consider the error dynamics (42), and stack the variables to form the overall state vector $e_i \in \mathbb{R}^6$. Define the vector fields

$$f_{\ell i}(e_i) = \begin{bmatrix} e_{2i} \\ \hbar_{\ell i}(e_{1i},e_{2i}) \end{bmatrix}, f_{vi}(e_i) = \begin{bmatrix} 0 \\ \hbar_{vi}(e_{1i},e_{2i}) \end{bmatrix}, \hat{f}_i(e) = \begin{bmatrix} 0 \\ \tilde{h}_i(e_{1i},e_{2i}) \end{bmatrix} \tag{47}$$

so that the full dynamics can be written as

$$\dot{e}_i = f_{\ell i}(e_i) + f_{vi}(e_i) + \hat{f}_i(e_i) \tag{48}$$

It follows that $f_{\ell i}$ is homogeneous with respect to r_ℓ with homogeneity degree $k_0 = -1 < 0$, and f_v is homogeneous with homogeneity degree $k_\infty = 1 > 0$. Define $e = \left[e_1^T, e_2^T, \cdots, e_{n_\Lambda}^T\right]^T, f_\ell(e) = \left[f_{\ell 1}^T, f_{\ell 2}^T, \cdots, f_{ln_\Lambda}^T\right]^T, f_v(e) = \left[f_{v1}^T, f_{v2}^T, \cdots, f_{vn_\Lambda}^T\right]^T$, $\hat{f}(e) = \left[\hat{f}_1^T, \hat{f}_2^T, \cdots, \hat{f}_{n_\Lambda}^T\right]^T$. Consider the system $\dot{e} = f_\ell(e)$ and choose $\eta > \max\{r_{\ell j}\}$. By [41], there exists a continuously differentiable, positive definite, proper function $V : \mathbb{R}^{6n_\Lambda} \to \mathbb{R}$ that is homogeneous of degree η with respect to r_ℓ, such that $L_{f_\ell}V$ is continuous negative definite and homogeneous of degree $\eta + k_0$.

Along $\dot{e} = f_\ell(e) + f_v(e) + \hat{f}(e)$, we obtain

$$\dot{V}(e) = L_{f_\ell}V(e) + L_{f_v}V(e) + L_{\hat{f}}V(e) = \sum_{j=1}^{n_\Lambda}\frac{\partial V}{\partial e_j}f_{\ell j} + \sum_{j=1}^{n_\Lambda}\frac{\partial V}{\partial e_j}f_{vj} + \sum_{j=1}^{n_\Lambda}\frac{\partial V}{\partial e_j}\hat{f} \tag{49}$$

For $e \in S^{n_\Lambda-1} = \left\{e \in \mathbb{R}^{6n_\Lambda} : \|e\| = 1\right\}$ and $\chi > 0$, using the given limits on $\tilde{h}_i$ and the homogeneity of V, we obtain

$$\sum_{i=1}^{n_\Lambda}\frac{\partial V}{\partial e_i}\lim_{\chi\to 0}\frac{\hat{f}_j(\chi^{r_{\ell 1}}e_{1i},\chi^{r_{\ell 1}}e_{2i})}{\chi^{k_0+\eta}} = 0, \tag{50}$$

for any $e \in S^{n_\Lambda-1}$.

Let $\lambda := \max_{e\in S^{n_\Lambda-1}}L_{\hat{f}}V(e)$, then $\lambda < 0$. There exists $\varepsilon_0 > 0$ such that for all $0 < \chi < \varepsilon_0$ and all $x \in S^{n_\Lambda-1}$, $\left|L_{\hat{f}}V(e)\right| = \left|\sum_{i=1}^{n_\Lambda}\frac{\partial V}{\partial e_i}\hat{f}_j(\chi^{r_{\ell 1}}e_{1i},\chi^{r_{\ell 1}}e_{2i})\right| \le \chi^{\eta+k_0}|\lambda|/2 \le \frac{|\lambda|\chi^{\eta+k_0}}{2m}V(e)$, where $m = \min_{e\in S^{n_\Lambda-1}}V(e) > 0$. Then, we have

$$\begin{aligned}\dot{V}(\chi^{r_\ell}e_1,\ldots,\chi^{r_\ell}e_{n_\Lambda}) =& \chi^{\eta+k_0}L_{f_l}V + L_{f_v}V(\chi^{r_\ell}e_1,\ldots,\varepsilon^{r_\ell}e_{n_\Lambda}) \\ &\times\left(L_{f_v}V\right)^{-1}(\chi^{r_v}e_1,\ldots,\chi^{r_v}e_{n_\Lambda})\times L_{f_g}V(\chi^{r_v}e_1,\ldots,\chi^{r_v}e_{n_\Lambda}) \\ &+L_{\hat{f}}V(\chi^{r_\ell}e_1,\ldots,\varepsilon^{r_\ell}e_{n_\Lambda}) \\ \le& \chi^{\eta+k_0}L_{f_l}V + \alpha_l\beta_l L_{f_g}V(\chi^{r_v}e_1,\ldots,\chi^{r_v}e_{n_\Lambda}) + \frac{|\lambda|\chi^{\eta+k_0}}{2m}V(e) \\ =& \chi^{\eta+k_0}L_{f_l}V + \alpha_l\beta_l\chi^{\eta+k_\infty}L_{f_g}V + \frac{|\lambda|\chi^{\eta+k_0}}{2m}V(e)\end{aligned} \tag{51}$$

where $\alpha_l = \max_{e\in S^{n_\Lambda-1}}L_{f_v}V(\chi^{r_\ell}e_1,\ldots,\varepsilon^{r_\ell}e_{n_\Lambda}), \beta_l = \max_{e\in S^{n_\Lambda-1}}\left(L_{f_v}V\right)^{-1}(\chi^{r_v}e_1,\ldots,\chi^{r_v}e_{n_\Lambda})$.

From Bhat and Bernstein [42], there exists $\varepsilon_1 = -\max_{\{z:V(z)=1\}}L_{f_\ell}V(e) > 0$, $\varepsilon_2 = -\max_{\{z:V(z)=1\}}L_{f_v}V(e)$ such that

$$L_{f_\ell}V(e) \le -\varepsilon_1[V(e)]^{\frac{\eta+k_0}{\eta}}, L_{f_v}V(e) \le -\varepsilon_2[V(e)]^{\frac{\eta+k_\infty}{\eta}} \tag{52}$$

Therefore, for every $e \in \mathbb{R}^{3n_\wedge}$, we have

$$\dot{V}(e) \le -\varepsilon_1[V(e)]^{\frac{\eta+k_0}{\eta}} - \varepsilon_2\alpha_l\beta_l[V(e)]^{\frac{\eta+k_\infty}{\eta}} + \frac{|\lambda|\chi^{\eta+k_0}}{2m}V(e) \tag{53}$$

According to Lemma 3, it follows that $V(e)$ achieves practical fixed time stability with the set

$$D = \begin{cases} \mathbb{R}^{3n_\wedge}, r < 1 \\ \left\{ e |\ V(e) \le k^\eta \left(\frac{\frac{|\lambda|\chi^{\eta-1}}{2m} - \sqrt{\left(\frac{|\lambda|\chi^{\eta-1}}{2m}\right)^2 - 4\varepsilon_1\varepsilon_2\alpha_l\beta_l}}{2\varepsilon_2\alpha_l\beta_l} \right)^\eta \right\}, r \ge 1 \end{cases} \tag{54}$$

and the settling time satisfies

$$T_2 \le \begin{cases} \frac{\eta}{\varepsilon_2\alpha_l\beta_l k_1}\left(\frac{\pi}{2} - \tan^{-1}k_2\right), r < 1 \\ \frac{\eta k}{(1-k)\sqrt{\varepsilon_1\varepsilon_2\alpha_l\beta_l}}, r \ge 1 \end{cases} \tag{55}$$

where $r = \frac{|\lambda|\chi^{\eta-1}}{4m\sqrt{\varepsilon_1\varepsilon_2\alpha_l\beta_l}} > 0, k \in (0,1), k_1 = \sqrt{\frac{4\varepsilon_1\varepsilon_2\alpha_l\beta_l - \delta_1^2}{4(\varepsilon_2\alpha_l\beta_l)^2}}, k_2 = -\frac{\delta_1}{\sqrt{4\varepsilon_1\varepsilon_2\alpha_l\beta_l - \delta_1^2}}, \delta_1 = \frac{|\lambda|\chi^{\eta+k_0}}{2m} = \frac{|\lambda|\chi^{\eta-1}}{2m}$. This completes the proof. □

Remark 2. *Decreasing α_2 accelerates the convergence speed near the equilibrium; however, when $\alpha_2 \in (0, 0.5)$, the marginal gain in the convergence rate becomes negligible while potentially increasing system chatter. Therefore, in practical applications and numerical simulations, the parameter α_2 is typically selected within the interval $[0.5, 0.9]$ to achieve a balance between dynamic performance and smooth control output. Furthermore, as $\alpha_2 \to 1^-$, the fractional power term $\mathrm{sig}(\cdot)^{\alpha_2}$ in controller (36) degenerates into a standard linear term. Because linear feedback control does not inherently support fixed-time convergence, the calculated settling-time upper bound $T_{\max}$ in Theorem 3 approaches infinity (i.e., $T_{\max} \to \infty$). Consequently, the closed-loop system stability degrades from fixed-time stability to asymptotic stability.*

4. Simulations

To verify the effectiveness of the proposed dynamic-trust-driven resilient formation control framework, numerical simulations are carried out for the multi-UAV system subjected to Sybil attacks and actuator input saturation. The networked system comprises one leader (labeled as 0), 12 legitimate followers, and 3 malicious nodes. Each malicious node fabricates neighbor identities and broadcasts falsified position and velocity states to the legitimate followers, thereby attempting to disrupt distributed coordination. Under the worst-case setting, each forged identity is assumed to be adjacent to all legitimate UAVs. The communication topology among the UAVs is illustrated in Figure 1.

The actuators of the UAVs are subject to saturation, with the maximum allowable overload given by $\eta_{\max} = 2.47$. Accordingly, the acceleration command generated by the outer-loop formation controller is restricted to the attitude-independent conservative bound $|\dot{v}_{ix}| \le 13.99, |\dot{v}_{iz}| \le 13.99, |\dot{v}_{iy} + g| \le 13.99$ m/s^2. The key parameters of the dynamic trust mechanism are selected as $\lambda = 0.2$, $a_{\max} = 1$, $k_\beta = 20$, and $d_{\min} = c_{\min} = 0.05$. The dynamic trust state is initialized as $\beta_{ij}(0) = 0$ for all links, which reflects the absence of any a priori trust evidence at the beginning of the mission. The physical-layer confidence metric $\sigma_{ij}(t) \in [0, 1]$ is generated following the radio-frequency fingerprinting method in [22]. Different attack onset times are used to distinguish the purposes of the simulation groups. In the first group, forged identities are introduced at 5 s, allowing a short pre-attack

reference interval and the subsequent evolution of the trust states, communication weights, and formation errors to be displayed in the same simulation. In the second and third groups, falsified-state injection starts at 35 s to separate the initial formation transient from the attack-induced response and examine resilience during formation maintenance.

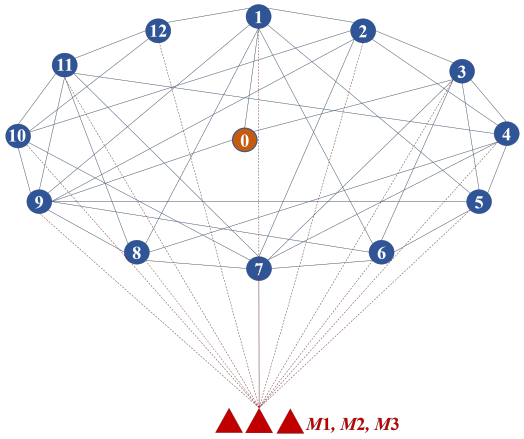


Figure 1. The communication topology among vehicles.

The first group of simulations is conducted to validate the dynamic trust updating rule established in Theorem 1. The objective is to examine whether the dynamic adjacency weighting mechanism governed by (4)–(6) can preserve the connectivity of the legitimate subgraph while progressively isolating the forged Sybil identities, so that resilient consensus is maintained in the presence of spoofing attacks and input saturation. In this scenario, the malicious node injects $n_{\text{syb}} = 3$ forged identities at $t = T_0 = 5\,\text{s}$. Both the 5 m deviation attack and the drift attack are evaluated.

Figure 2 depicts the evolution of the dynamic adjacency weights. The weights associated with legitimate links, initially set to the nominal value $a_{\max}$, rapidly converge to a neighborhood of $a_{\max}$. In contrast, the weights associated with links originating from Sybil identities decrease monotonically from $a_{\max}$ toward zero. This decay is caused by the accumulation of negative evidence in the trust state $\beta_{im}(t)$. The result reveals that legitimate connectivity is preserved while the malicious links are isolated.

The trust state $\beta_{ij}(t)$ itself is illustrated in Figure 3. For the legitimate links, $\beta_{ij}(t)$ increases from zero and settles in a small neighbourhood of the theoretical steady value $d_{\min}/\lambda = 0.25$, whereas for the Sybil links it decreases and settles near $-c_{\min}/\lambda = -0.25$. Figure 4 illustrates the evolution of the formation errors. After the attack is launched at $t = T_0$, omitting trust weights or directly switching the weights based on the confidence metric in [22] leads to enlarged formation errors. In contrast, under the proposed dynamic trust method, the trust weights associated with Sybil links gradually decay. Consequently, the influence of falsified information is progressively attenuated, and the formation errors converge to a neighborhood of the origin.

To evaluate the effect of the mapping gain, we compare the isolation time and the peak $|\dot{a}_{ij}|$ for $k_\beta = 5, 10, 20, 40$, while keeping all other settings unchanged. The isolation time is defined as the duration required for the malicious link weights to stay below the threshold 0.02 over the remaining observation interval, rather than the time needed for the weights to reach exactly zero. The peak weight-change rate is computed from the filter dynamics and the mapping derivative, taking into account the derivatives on both sides of the sampling instants. The simulation results for the isolation time are shown in Figure 5, and those for the peak weight-change rate are shown in Figure 6. The gain k_β determines the steepness of the mapping from the trust state to the communication weights. For a finite k_β, this mapping is continuous. Increasing k_β can reduce the isolation time; however, a larger gain also narrows

the transition region near the zero-trust state, which may lead to approximately switch-like weight variations. Therefore, the gain should be chosen by jointly considering the target weight, the probabilistic safety margin, and the practical weight change rate, rather than relying solely on the continuity or saturation behavior of the mapping.

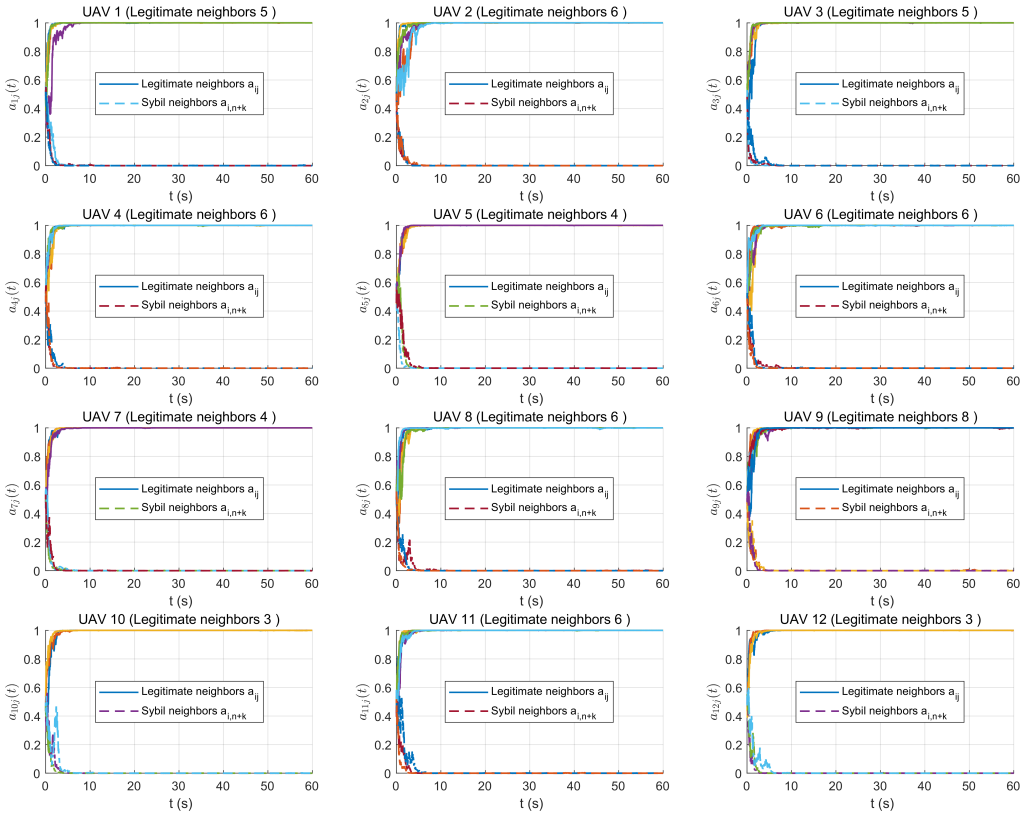


Figure 2. The evolution of the dynamic adjacency weights with $k_\beta = 20$.

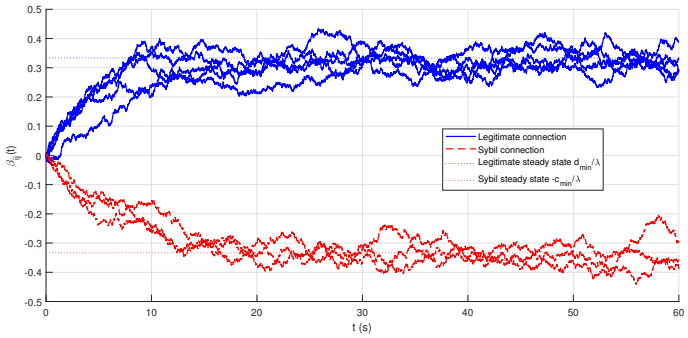


Figure 3. The trust state $\beta_{ij}(t)$.

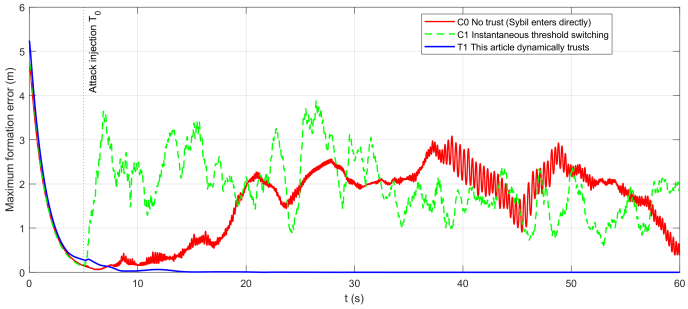


Figure 4. The evolution of the formation errors.

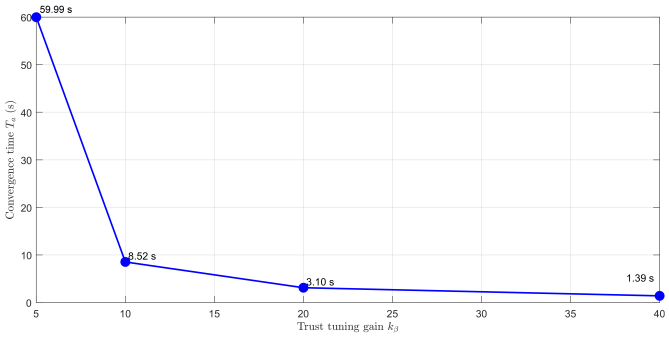


Figure 5. The isolation time with $k_\beta = 5, 10, 20, 40$.

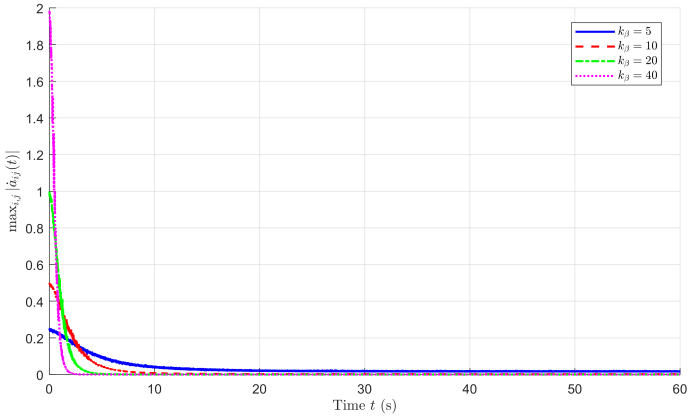


Figure 6. The peak weight-change rate $\left|\dot{a}_{ij}\right|$.

The second group of simulations is devoted to verifying the finite-time resilient formation controller proposed in Theorem 2. The objective is to demonstrate that, under the simultaneous effects of the Sybil attack and the input saturation constraint, the legitimate followers can track the leader's trajectory and establish the desired geometric formation within a finite time. The finite-time control parameters in (17) are $\alpha_1 = 0.8, \alpha_2 = 2\alpha_1/(1+\alpha_1)$, $k_1 = 9, k_2 = 1.4$, and the saturation thresholds $\gamma_1 = 1.6, \gamma_2 = 2$. Choose $\rho = 0.05$, $c = 0.3$. The initial positions and velocities of the follower UAVs are randomly generated around the leader to emulate uncertainties during the initial deployment process. Figure 7 presents the three-dimensional flight trajectories of the leader and the followers. Starting from the randomized initial positions, the followers gradually adjust their positions relative to the leader and eventually settle at the prescribed offsets, so that the desired formation geometry is established. The state-tracking and tracking-error results are shown in Figures 8 and 9, respectively. Figures 8 and 9 indicate that the legitimate follower UAVs accurately track the leader's position and velocity states. The tracking errors decrease rapidly from their initial values and converge to a small neighborhood of the origin within 18.53 s, where they remain thereafter. Although a Sybil attack is launched at $T = 35$ s, during which malicious nodes inject forged state information, its impact remains limited after the trust weights have accumulated sufficient evidence. Following the transient response, the formation is maintained without noticeable distortion. Figure 10 presents the time histories of the control inputs. The control-input magnitudes remain within the prescribed bounds throughout the simulation. These results demonstrate that the proposed control algorithm effectively prevents actuator overload that may arise from an increased number of neighbors in the consensus protocol.

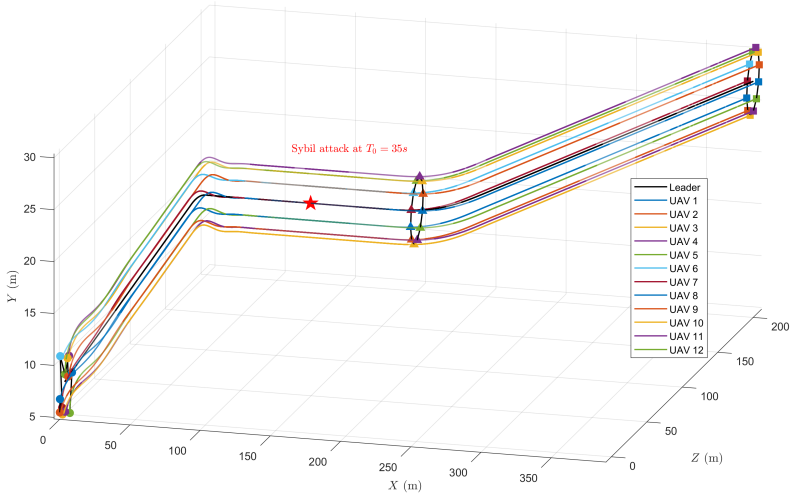


Figure 7. Three-dimensional flight trajectories under finite-time formation control. Small triangles and squares represent the position of the drone, large circles represent the formation shape, and pentagrams represent the start time of the attack

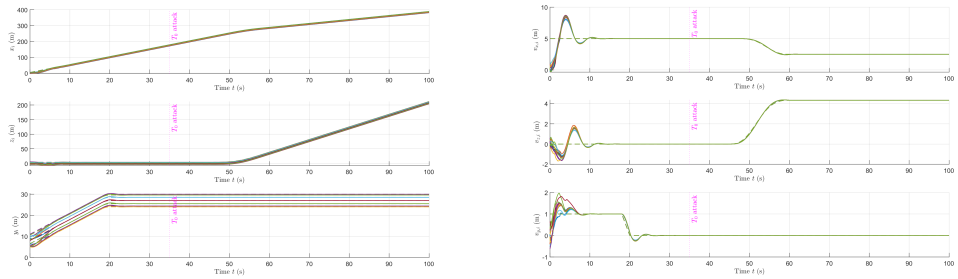


Figure 8. Position and velocity tracking of the follower UAVs.

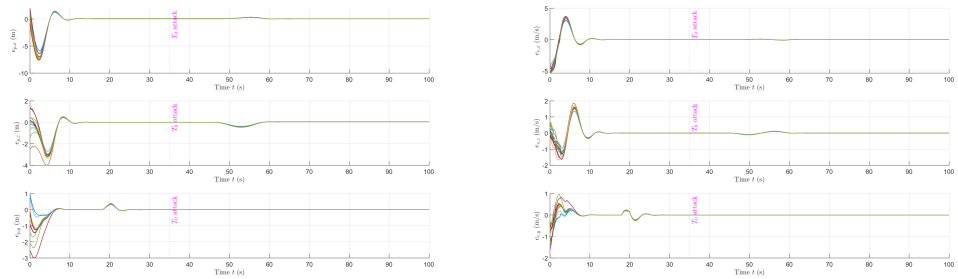


Figure 9. Position and velocity tracking errors of the follower UAVs.

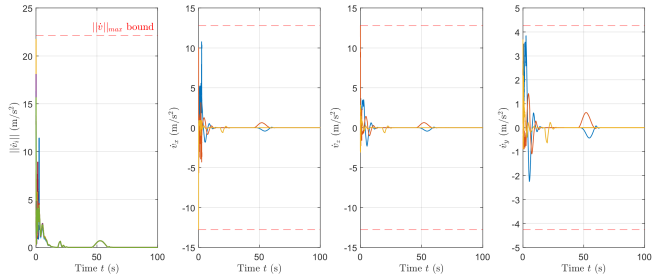


Figure 10. The control input of the follower UAVs with the finite-time control algorithm.

The third group of simulations is carried out to verify the fixed-time resilient formation controller proposed in Theorem 3. Figure 11 illustrates the three-dimensional flight trajectories of the leader and follower UAVs. Starting from randomly generated initial positions, the followers gradually adjust their relative positions with respect to the leader and converge

to the prescribed formation offsets, thereby establishing the desired formation geometry. The fixed-time control parameters in (36) are $\alpha_2 = 0.8$, $\alpha_1 = \alpha_2/(2-\alpha_2) = 0.667$, $\tilde{\alpha}_1 = (4-3\alpha_2)/(2-\alpha_2)$, $\tilde{\alpha}_2 = (4-3\alpha_2)/(3-2\alpha_2)$, $h_{1x} = h_{1z} = 3, h_{2x} = h_{2z} = 3.5$, $h'_{1x} = h'_{1z} = 2.5, h'_{2x} = h'_{2z} = 2.5$, and $\gamma_2 = 2$, $h_{1y} = 1.05, h_{2y} = 1, h'_{1y} = 1.05, h'_{2y} = 1$, and $\gamma_2 = 2$. This parameter selection ensures that constraint (37) holds, because law (36) normalizes the per-neighbor tanh gains by $(n+1)$. As a result, the command ceiling is independent of the neighbor count. The state-tracking and tracking-error results are shown in Figures 12 and 13, respectively. These results demonstrate that the legitimate follower UAVs accurately track the leader's position and velocity states. The tracking errors decrease rapidly from their initial values and converge to a small neighborhood of the origin within 26.68 s, where they remain thereafter. Although a Sybil attack is launched at $T = 35$ s, during which malicious nodes inject falsified state information, its effect remains limited once the trust weights have accumulated sufficient evidence. Following the transient response, the desired formation is maintained without noticeable distortion. Figure 14 presents the time histories of the control inputs. The control-input magnitudes remain within the prescribed bounds throughout the simulation, demonstrating that the proposed control algorithm (36) effectively prevents actuator overload that may arise as the number of neighbors in the consensus protocol increases.

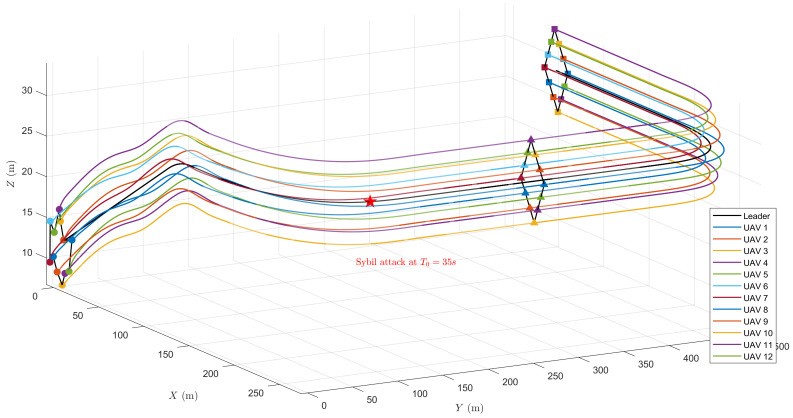


Figure 11. Three-dimensional flight trajectories under fixed-time formation control. Small triangles and squares represent the position of the drone, large diamonds represent the formation shape, and pentagrams represent the start time of the attack.

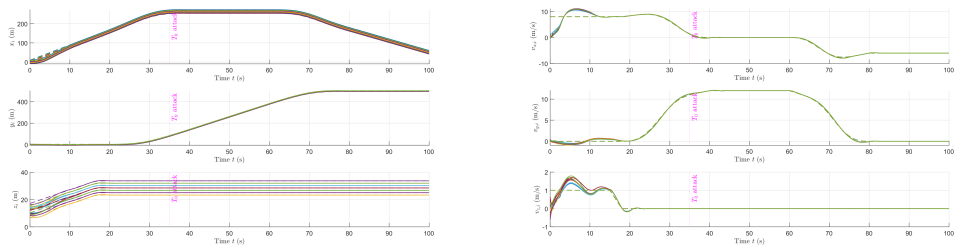


Figure 12. Position and velocity tracking of the followers under the control algorithm (36).

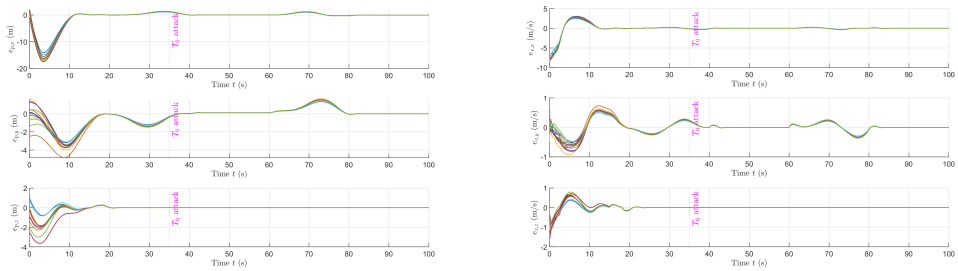


Figure 13. Position and velocity tracking errors of the followers under the control algorithm (36).

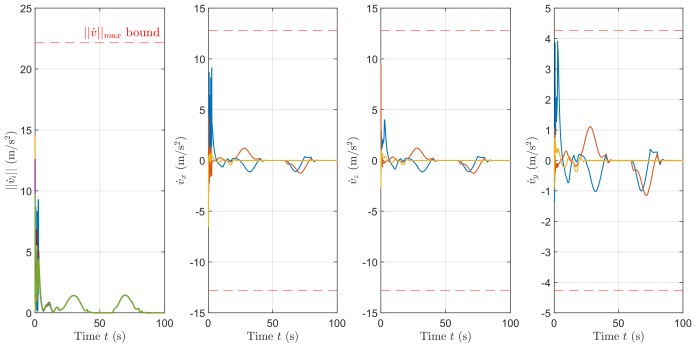


Figure 14. The control input of the follower UAVs with the fixed-time control algorithm.

In summary, the above examples demonstrate that the dynamic trust mechanism, together with the finite-time and fixed-time formation controllers, enables the UAVs to track the leader's trajectory and achieve the desired subformation patterns within a limited time. The proposed approach effectively accomplishes various tasks in the presence of Sybil attacks and input-saturation constraints.

5. Conclusions

This paper developed a dynamic trust-driven resilient formation control framework for multi-UAV systems subject to Sybil attacks and actuator saturation. A confidence-based dynamic trust mechanism was introduced to adaptively assign communication weights, thereby maintaining the connectivity of the legitimate UAV subgraph and attenuating the effect of Sybil links. On this basis, distributed finite-time and fixed-time saturated formation controllers were designed. The former guarantees finite-time formation tracking, whereas the latter provides a practical fixed-time convergence bound for initial tracking errors belonging to a prescribed compact set. Lyapunov-based and homogeneity analyses established the corresponding stability and input-boundedness properties. Simulation results verify that the proposed method effectively mitigates Sybil-induced communication disturbances and achieves accurate formation tracking without violating actuator limits. These results demonstrate the applicability of the proposed framework to resilient cooperative control of networked UAVs under coupled communication-security and actuation constraints.

Author Contributions: Conceptualization, H.W. and T.L.; methodology, H.W.; software, T.L.; formal analysis, H.W., C.H. and D.Z.; investigation, T.L.; resources, C.H.; writing—original draft preparation, C.H.; writing—review and editing, D.Z.; visualization, T.L.; funding acquisition, D.Z. All authors have read and agreed to the published version of the manuscript.

Funding: This research was funded by the National Key R&D Program of China under Grant 2022YFB3104300.

Data Availability Statement: The original contributions presented in this study are included in the article. Further inquiries can be directed to the corresponding authors.

Conflicts of Interest: Mr. Hanghang Wang and Mr. Tangxing Liu were employed by the Nanjing Research Institute of Electronic Engineering, Nanjing, China, which is affiliated with China Electronics Technology Group Corporation (CETC). The remaining authors declare that the research was conducted in the absence of any commercial or financial relationships that could be construed as a potential conflict of interest.

References

1. Alqudsi, Y.; Makaraci, M. Exploring advancements and emerging trends in robotic swarm coordination and control of swarm flying robots: A review. *Proc. Inst. Mech. Eng. Part C J. Mech. Eng. Sci.* **2025**, *239*, 180–204. [CrossRef]
2. Zhang, J.; Qu, Q.; Chen, X. Understanding collective behavior in biological systems through potential field mechanisms. *Sci. Rep.* **2025**, *15*, 3709. [CrossRef] [PubMed]
3. Wang, S.; Yan, S.; Shi, L.; Zhu, P. Multi-agent flocking with asynchronous cooperative-competitive interactions. *J. Frankl. Inst.* **2026**, *363*, 108392. [CrossRef]
4. Khaledi, M.; Kiumarsi, B. Data-Driven Distributed Safe Control Design for Multi-Agent Systems. *Int. J. Adapt. Control Signal Process.* **2026**, *40*, 137–150. [CrossRef]
5. Pantelimon, G.; Tepe, K.; Carriveau, R.; Ahmed, S. Survey of multi-agent communication strategies for information exchange and mission control of drone deployments. *J. Intell. Robot. Syst.* **2019**, *95*, 779–788. [CrossRef]
6. Rajchakit, G.; Tajudeen, M.M.; Banu, K.A.; Lim, C.P.; Tatar, N.E.; Huang, T. Learnable-order fractional recurrent networks: Structured identification of memory in non-stationary sequences. *Neural Netw.* **2027**, *205*, 109537. [CrossRef] [PubMed]
7. Zhang, A.; Zhou, D.; Yang, P.; Yang, M. Event-triggered finite-time consensus with fully continuous communication free for second-order multi-agent systems. *Int. J. Control Autom. Syst.* **2019**, *17*, 836–846. [CrossRef]
8. Zhou, D.; Chen, P.; Cao, Z.; He, C.; Han, X.; Niu, Y. Finite-and fixed-time privacy-preserving formation control for multiple quadrotor systems with input delay and connectivity maintenance. *ISA Trans.* **2026**, *168*, 515–530. [CrossRef] [PubMed]
9. Tajudeen, M.M.; Asmiya Banu, K.; Tatar, N.E.; Rajchakit, G.; Lim, C. Non-fragile event-triggered control for IT2 fuzzy multi-weighted complex networked system with time-varying coupling delay subject to multiple attacks. *Int. J. Syst. Sci.* **2026**, 1–19. [CrossRef]
10. Suresh, M.; Samidurai, R.; Tajudeen, M.H.M.; Alharthi, M.; Alsulami, I.M.; Alghamdi, N.A. Finite-Time Global Mittag-Leffler Projective Synchronization of Uncertain Fractional-Order Delayed Neural Networks with Heterogeneous Fractional Orders via Integral Sliding Mode Control. *Mathematics* **2026**, *14*, 2987. [CrossRef]
11. Kabir, M.H.; Razib, M.; Jahin, Z.; Jesan, Z. Zero Trust Based Critical Infrastructure Cybersecurity Framework with AI-Driven Threat Detection and Secure Network Modernization. *J. Comput. Sci. Technol. Stud.* **2026**, *8*, 1–14. [CrossRef]
12. Zhou, L.; Luo, Z.; Shi, J. DQN-ALNS for UAV Reconnaissance Routing Problem with Target Priority Consideration. *Tsinghua Sci. Technol.* **2026**, *31*, 274–290. [CrossRef]
13. Chulerttiyawong, D.; Jamalipour, A. Sybil attack detection in internet of flying things-ioft: A machine learning approach. *IEEE Internet Things J.* **2023**, *10*, 12854–12866. [CrossRef]
14. Yemini, M.; Nedić, A.; Goldsmith, A.J.; Gil, S. Resilient Distributed Optimization for Multiagent Cyberphysical Systems. *IEEE Trans. Autom. Control* **2025**, *70*, 3952–3967. [CrossRef]
15. Yu, A.; Kolotylo, I.; Hashim, H.A.; Eltoukhy, A.E.E. Electronic Warfare Cyberattacks, Countermeasures, and Modern Defensive Strategies of UAV Avionics: A Survey. *IEEE Access* **2025**, *13*, 68660–68681. [CrossRef]
16. Cui, Y.; Zhang, Q.; Feng, Z.; Zhou, Y.; Wei, Z.; Zhang, P.; Peng, J. Seeing Is Believing: Detecting the Sybil Attacks in FANETs by Mapping Visual and Auditory Domains. *IEEE Trans. Veh. Technol.* **2026**, *75*, 9825–9840. [CrossRef]
17. Dong, M.; Sheng, D. Research progress on cyber-physical power system security: Threat modeling paradigms, key defense technologies, and system resilience evolution. *Adv. Resour. Res.* **2026**, *6*, 697–740.
18. Tajudeen, M.M.; Banu, K.A.; Muslikh, M.; Rajchakit, G.; Hassaballa, A.A.; Lim, C.; Jaghdam, I.H. Adaptive event-driven synchronisation control for Lur'e chaotic systems facing actuator faults subject to hybrid attacks. *Int. J. Syst. Sci.* **2026**. [CrossRef]
19. Zhou, D.; Bo, L.; Liu, S.; Xin, Y.; Cao, J.; Fu, X. A Multi-View Hierarchical Intrusion Detection Model with Integrating Spatiotemporal Feature for Industrial Control System. *Tsinghua Sci. Technol.* **2026**, *31*, 1778–1801. [CrossRef]
20. Tajudeen, M.M.; Banu, K.A.; Tatar, N.e.; Rajchakit, G.; Huang, T. Observer based security control for interval type-2 fuzzy networked system subject to hybrid attacks via resilient event-triggered scheme and Its application. *J. Frankl. Inst.* **2026**, *363*, 108777. [CrossRef]
21. Benaly, M.; El Mrabet, A.; El Karch, H.; El Gouri, R.; Mezouari, A.; Hlou, L. Sharif: Edge Computing and Energy Consumption Optimization for UAVs at Various Altitudes. *Eng. Technol. Appl. Sci. Res.* **2026**, *16*, 30774–30780. [CrossRef]
22. Gil, S.; Kumar, S.; Mazumder, M.; Katabi, D.; Rus, D. Guaranteeing spoof-resilient multi-robot networks. *Auton. Robot.* **2017**, *41*, 1383–1400. [CrossRef]
23. Zhang, Y.; Dang, Y.; Kaveh, M.; Yan, Z.; Jäntti, R.; Han, Z. Physical Layer Challenge-Response Authentication Between Ambient Backscatter Devices. *IEEE Trans. Inf. Forensics Secur.* **2026**, *21*, 1512–1527. [CrossRef]
24. Faisal, I.A.; Purboyo, T.W.; Ansori, A.S.R. A review of accelerometer sensor and gyroscope sensor in IMU sensors on motion capture. *J. Eng. Appl. Sci.* **2019**, *15*, 826–829. [CrossRef]
25. Homaeinezhad, M.R.; Alvar, M.M.M.; Soordi, A.; Aghaei, M.; Hatefikousha, A.; Charehjoo, T. Solution to Asymptotic Stability in Tracking Control of Nonlinear Systems With Control Input Differentiation, Actuator Dynamics, and Saturation Constraints. *IET Control Theory Appl.* **2026**, *20*, e70108. [CrossRef]

26. Qi, G.; Su, H.; Gao, Y. Distributed Safety Control for Fixed-Wing UAV Swarms within a 3D Virtual Tube via Control Barrier Functions. *Unmanned Syst.* **2026**. [CrossRef]
27. Yang, H.; Yu, Z.; Fu, M.; Zhang, Y. Resilient Consensus Control for Multiple UAVs With Input Saturation Under DoS Attacks. *IEEE Trans. Cybern.* **2025**, *55*, 1159–1171. [CrossRef] [PubMed]
28. Zhao, S.; Zheng, J.; Yi, F.; Wang, X.; Zuo, Z. Exponential Predefined Time Trajectory Tracking Control for Fixed-Wing UAV with Input Saturation. *IEEE Trans. Aerosp. Electron. Syst.* **2024**, *60*, 6406–6419. [CrossRef]
29. Zhu, G.; Lv, L.; Sun, L.; Zhang, X. Distributed dynamic surface control for a class of quadrotor uavs with input saturation and external disturbance. *Drones* **2024**, *8*, 77. [CrossRef]
30. Li, J.; Liu, Y.; Yu, J. Observer-based decentralized dynamic event-triggered scheme and resilient control under DoS attacks. *Trans. Inst. Meas. Control* **2025**, *47*, 2663–2675. [CrossRef]
31. Beikbabaei, M.; Mehrizi-Sani, A.; Liu, C.C. State-of-the-art of cybersecurity in the power system: Simulation, detection, mitigation, and research gaps. *IET Gener. Transm. Distrib.* **2025**, *19*, e70006. [CrossRef]
32. Yang, S.N.; Guo, L.D.; Huang, S.J. Observer-based PID quasi-consensus control of stochastic multi-agent systems under multimodal false data injection attacks. *Neurocomputing* **2026**, *675*, 132941. [CrossRef]
33. Zhou, D.; He, L.; Cao, Z.; Zhang, A.; Han, X. Event–Triggered Fixed–Time Resilient Control for Mobile Sensor Networks with a Sybil Attack and Input Delay. *Int. J. Appl. Math. Comput. Sci.* **2025**, *35*, 129–142. [CrossRef]
34. Chen, J.; Shi, Y. Stochastic model predictive control framework for resilient cyber-physical systems: Review and perspectives. *Philos. Trans. R. Soc. A* **2021**, *379*, 20200371. [CrossRef] [PubMed]
35. Zhuang, J.; Peng, S.; Peng, H. Finite-time and fixed-time consensus of nonlinear multi-agent systems: A unified two-phase control. *Int. J. Robust Nonlinear Control* **2024**, *34*, 9438–9455. [CrossRef]
36. Zhou, D.; Zhang, A.; Yang, P. Fixed-time event-triggered consensus of second-order multi-agent systems with fully continuous communication free. *IET Control Theory Appl.* **2020**, *14*, 2385–2394. [CrossRef]
37. Garg, K.; Panagou, D. Characterization of Domain of Fixed-time Stability under Control Input Constraints. In *Proceedings of the 2021 American Control Conference (ACC)*; IEEE: Piscataway, NJ, USA, 2021; pp. 2272–2277.
38. Zhang, D.; Duan, G. Leader-following fixed-time output feedback consensus for second-order multi-agent systems with input saturation. *Int. J. Syst. Sci.* **2018**, *49*, 2873–2887. [CrossRef]
39. Bu, Y.; Yan, Y.; Yang, Y. Advancement challenges in UAV swarm formation control: A comprehensive review. *Drones* **2024**, *8*, 320. [CrossRef]
40. Yang, P.; Zhang, A.; Zhou, D. Event-triggered finite-time formation control for multiple unmanned aerial vehicles with input saturation. *Int. J. Control Autom. Syst.* **2021**, *19*, 1760–1773. [CrossRef]
41. Rosier, L. Homogeneous Lyapunov function for homogeneous continuous vector field. *Syst. Control Lett.* **1992**, *19*, 467–473. [CrossRef]
42. Bhat, S.P.; Bernstein, D.S. Geometric homogeneity with applications to finite-time stability. *Math. Control Signals Syst.* **2005**, *17*, 101–127. [CrossRef]

Disclaimer/Publisher's Note: The statements, opinions and data contained in all publications are solely those of the individual author(s) and contributor(s) and not of MDPI and/or the editor(s). MDPI and/or the editor(s) disclaim responsibility for any injury to people or property resulting from any ideas, methods, instructions or products referred to in the content.